Available online at www.sciencedirect.com
ScienceDirect
Vision Research xxx (2006) xxx–xxx
Vision Research
www.elsevier.com/locate/visres

Detection of Gabor patterns of different sizes, shapes, phases and eccentricities

John M. Foley [a,*], Srinivasa Varadharajan [a,1], Chin C. Koh [b], Mylene C.Q. Farias [b]

[a] Department of Psychology, University of California, Santa Barbara, CA 93106, USA
[b] Department of Electrical and Computer Engineering, University of California, Santa Barbara, CA 93106, USA

Received 31 March 2006; received in revised form 30 August 2006

Abstract

Contrast thresholds of vertical Gabor patterns were measured as a function of their eccentricity, size, shape, and phase using a 2AFC method. The patterns were 4 c/deg and they were presented for 90 or 240 ms. Log thresholds increase linearly with eccentricity at a mean rate of 0.47 dB/wavelength. For patterns centered on the fovea, thresholds decrease as the area of the pattern increases over the entire standard deviation range of 12 wavelengths. The TvA functions are concave up on log–log coordinates. For small patterns there is an interaction between shape and size that depends on phase. Threshold contrast energy is a U-shaped function of area with a minimum in the vicinity of 0.4 wavelength indicating detection by small receptive fields. Observers can discriminate among patterns of different sizes when the patterns are at threshold indicating that more than one mechanism is involved. The results are accounted for by a model in which patterns excite an array of slightly elongated receptive fields that are identical except that their sensitivity decreases exponentially with eccentricity. Excitation is raised to a power and then summed linearly across receptive fields to determine the threshold. The results are equally well described by an internal-noise-limited model. The TvA functions are insufficient to separately estimate the noise and the exponent of the power function. However, an experiment that shows that mixing sizes within the trial sequence has no effect on thresholds, suggests that the limiting noise does not increase with the number of mechanisms monitored.

Keywords: Contrast; Threshold; Receptive field; Size; Models

1. Introduction

Gabor patterns have become widely used in vision research. Consequently, it is desirable to have accurate measurements of sensitivity to Gabor patterns of different sizes, shapes and phases. Such measurements may also contribute to estimating the properties of the receptive fields of human pattern vision mechanisms and the way in which mechanism signals combine to determine thresholds.

There have been many attempts to use psychophysics to determine the receptive fields of the detecting mechanisms. These go back to early measurements of spatial summation. Graham, Brown, and Mote (1939) proposed an explicit model of spatial summation for uniform patches of light, which was in essence a model of the receptive field of the detecting unit. After it became known that receptive fields contain both excitatory and inhibitory regions, a paradigm introduced by Westheimer (1967) came into use. In the Westheimer paradigm a small spot was flashed in the center of a steady disk. As the diameter of the disk increased, the threshold for the flash increased and then decreased. The size at which the threshold reached maximum was taken to be the size of the excitatory region of the detecting field and the size at which the threshold ceased to decrease was taken to be the size of the inhibitory region. Later studies made the context pattern subthreshold and flashed it with the target to minimize adaptation. This came to be called the method of subthreshold

* Corresponding author. Fax +1 805 893 4303.
E-mail address: foley@psych.ucsb.edu (J.M. Foley).
[1] Present address: Elite School of Optometry, Chennai 600 016, India.

0042-6989/$ - see front matter © 2006 Elsevier Ltd. All rights reserved.
doi:10.1016/j.visres.2006.09.005

summation. Some studies used a line as a target with context lines on either side (Hines, 1976). Many studies were done involving subthreshold summation of gratings. A common paradigm was to reduce the separation between two grating frequencies until linear summation of their effects was obtained. This was shown to be a poor method for estimating the bandwidth of the underlying fields due to complications produced by probability summation (Graham & Robson, 1987). On the assumption that pattern adaptation reduces the sensitivity of receptive fields that respond to the pattern, bandwidths were estimated from adaptation effects by Blakemore and Campbell (1969) and Georgeson and Harris (1984) to be about 1.4 octaves. However, the desensitization model that they used is not a completely adequate account of adaptation (Foley & Chen, 1997). Legge and Foley (1980) and Wilson et al. (1983) used pattern masking to estimate bandwidth. Both studies used a model of masking that assumed that masking depends on the excitation of the detecting field by the mask. It is now clear that masking depends on inhibition produced by the mask and this inhibition is more broadly tuned than is the excitation of the detecting mechanism (Foley, 1994). Further, it is now known that the extent of the mask beyond the target can have a large effect on the magnitude of masking (Yu & Levi, 1997, 1998). Although there are now models that incorporate lateral context effects (Chen & Tyler, 2001; Varadharajan & Foley, 2003; Yu, Klein, & Levi, 2003), none of these newer models is completely satisfactory and none has been used to estimate receptive fields.

Absolute threshold experiments offer another way to find out about pattern mechanisms. There have been numerous studies of absolute contrast thresholds for patterns, some of which have sought to determine the nature of the detecting mechanisms. There is some evidence for receptive fields matched to the stimulus pattern (Hauske, Wolf, & Lupp, 1976; Rovamo, Luntinen, & Nasanen, 1993), even when the pattern is a sharply truncated Gabor pattern (Syvajarvi, Nasanen, & Rovamo, 1999), but other results are inconsistent with these. The evidence generally points to Gabor-like receptive fields, but estimates of their size or shape differ greatly. Most models have used circular Gabor receptive fields that are relatively small, and there is evidence that such fields mediate detection (Watson, Barlow, & Robson, 1983). However, Polat and Tyler (1999) have presented evidence of detection by receptive fields that are greatly elongated in the direction parallel to the stripes. In addition to the shape issue, there is also a lack of agreement about the size of these fields and whether there is more than one size tuned to the same spatial frequency. In practice, our ability to use detection experiments to determine receptive fields depends on the level of accuracy and precision in threshold measurement that can be attained.

The extraction of receptive field estimates from such measurements is fraught with difficulties. The principal difficulty is that for most patterns many different receptive fields are likely to contribute to detection and these fields may vary with the size of the pattern. For example, narrow patterns contain a wide range of spatial frequencies and may stimulate receptive fields tuned to very different spatial frequencies. Large patterns undoubtedly stimulate many receptive fields in different retinal locations, and these may differ in spatial sensitivity.

Our approach is as follows. Our stimuli are Gabor patterns. They have the same form as the two-dimensional Gabor functions that have been shown to describe the spatial sensitivity functions of V1 neurons in monkeys (Ringach, 2002). Their center spatial frequency (4 c/deg) is close to the frequency to which the system is most sensitive at the luminance that we used. This increases the likelihood that receptive fields tuned near to this frequency will detect the patterns. We test this hypothesis by fitting a model based on Gabor receptive fields to our data. We find that a model containing a spatial array of Gabor receptive fields tuned to our pattern frequency, whose responses are power functions of their excitation and are summed linearly, gives a good account of our results.

In addition to varying the size and shape of the patterns, we have varied spatial phase relative to the center of the pattern. We find that for small patterns phase interacts with size and this interaction depends on phase. The model accounts for this effect as well. We also performed related experiments on the effect of eccentricity on thresholds, size discrimination at threshold, and the effect of mixing different sizes of patterns within a block of trials.

2. Background

2.1. Effect of size

There have been many studies of contrast thresholds for sinewave gratings as a function of size. In a 1996 review Garcia-Perez and Sierra-Vazquez (1996) counted 36 such experiments and there have been more since then. Most of these used rectangularly windowed sinewave gratings that varied in width in the direction orthogonal to the bars. A few used circular, square or Gaussian windows. Studies of size effects are consistent in showing that for most spatial frequencies, the threshold decreases as size increases. For small sizes the decrease is rapid, but as size increases the threshold decreases more slowly, appearing to approach an asymptote for large sizes. Using grating patches, Robson and Graham (1981) found an increase in sensitivity out to at least 16 wavelengths in the fovea. There are exceptions to this form at very low and very high spatial frequencies (Pointer & Hess, 1989). Some authors have used two straight line segments to describe the data when plotted on log–log coordinates (Kersten, 1984; Polat & Tyler, 1999).

A Gabor pattern is produced by multiplying a sinewave grating by a two-dimensional Gaussian function. For Gabor patterns the description of experimental results is complicated by the several different measures that are used

Please cite this article in press as: Foley, J. M. et al., Detection of Gabor patterns of different sizes, ..., *Vision Research* (2006), doi:10.1016/j.visres.2006.09.005

for the extent (spread) of these functions. The relations among these are described by Graham (1989, Table 2.1). We will use the standard deviation, which is the smallest and the most familiar of these measures. Only a few studies have used Gaussian windows. Kersten (1984) used sine-waves with one-dimensional Gaussian envelopes orthogonal to the grating orientation and a wide range of standard deviations as small as 0.04 cycle. Kersten found thresholds to decrease for standard deviations up to at least 1.4 cycles and the decrease was roughly linear on log–log coordinates in most conditions.

There are a few studies that measure threshold for elliptical Gabor patterns as a function of their length and width. Watson et al. (1983), Anderson and Burr (1991) and Polat and Tyler (1999) are the principal studies. Watson et al. measured thresholds for Gabor patterns that varied in spatial frequency, length and width, temporal frequency and duration. They point out that, if detection is mediated by a single detector that sums excitation linearly, the contrast energy threshold will be minimum when the stimulus waveform matches the weighting function of the receptive field. They present their data in graphs of energy threshold vs. the parameters of the stimulus pattern. Although they report only a few of their measurements on a single observer, they conclude from a larger data set that the minimum threshold occurs at a standard deviation of about 1 wavelength in both height and width, a duration of 160 ms and a drift rate of 4 Hz. The optimum spatial frequency was found to lie between 6 and 8 c/deg at their background luminance of 340 cd/m^2. Their inference of the properties of the detector from contrast energy thresholds depends on the assumption that a single linear detector determines the threshold.

Anderson and Burr (1991) measured thresholds for Gabor patterns drifting at 8 Hz. They varied length and width in separate experiments, with the fixed dimension equal to 1.5 cycles. They fitted a model with elliptical Gabor receptive fields and probability summation and estimated the standard deviations in wavelengths in both directions. These increase with spatial frequency from 0.065 wavelength at 0.1 c/deg to 0.25 wavelength at 10 c/deg.

Polat and Tyler (1999) found that the threshold for a Gabor pattern depends strongly on the shape of the envelope, decreasing much more with area for patterns elongated parallel to the grating than for those elongated perpendicular to the grating or for patterns with circular envelopes. They conclude that maximal detection efficiency is achieved for standard deviations that average about 2.8 grating cycles in length and about 0.43 wavelengths in width.

These studies show that there is quite a bit of inconsistency in results with respect to how the threshold depends on the size and shape of Gabor patterns and the implications for the size and shape of the receptive fields that mediate detection.

2.2. Effect of eccentricity

It is known that sensitivity to patterns decreases as a function of eccentricity. Since this effect places an important constraint on models of the effect of size, we examined it first. Robson and Graham (1981) measured contrast thresholds for a 4-cycle patch of horizontal grating presented at eccentricities of 0–32 wavelengths above and below the fixation point. They found that the log threshold increases approximately linearly with eccentricity with a slope of about 0.4 dB/wavelength (4.5%/wavelength). This means that sensitivity is falling off exponentially with eccentricity. Pointer and Hess (1989) used circular horizontal Gabor patterns with standard deviations of 2.27 wavelengths that were counterphase modulated at 1 Hz. They measured thresholds in horizontal and vertical meridians and used a wider range of spatial frequencies. They also found that the log threshold increases approximately linearly with eccentricity. The slope depended on the meridian, being about 0.5 dB/wavelength for the vertical meridian and 0.33 dB/wavelength for the horizontal meridian for spatial frequencies >1 c/deg. For spatial frequencies of 0.2–0.8 c/deg the rate of sensitivity decrease with eccentricity was about double these values.

3. Our study

Our study consisted of four experiments. In the first we measured the contrast threshold of a Gabor pattern as a function of its eccentricity. Its goal was to provide measurements of the eccentricity effect made under the same conditions as our other experiments. These provide a constraint on models of the effect of size. In the second experiment we measured contrast thresholds as a function of size, shape and phase for three classes of Gabor patterns: circular, collinearly varying (patterns whose standard deviation in the direction collinear with the stripes varies), and orthogonally varying (patterns whose standard deviation in the direction orthogonal to the stripes varies). All three sets of pattern shapes were created with each of three phases re the center of the pattern: sine, cosine, and anti-cosine, producing nine pattern sets. All the patterns were centered on the fixation point. Here our goal was both to determine the thresholds for these patterns and to use them as a basis for models of pattern detection. The third experiment measured the discrimination of circular Gabor patterns of different sizes when their contrasts were at threshold. This was a direct test of the hypothesis that multiple receptive fields underlie the detection of large patterns. The fourth experiment measured thresholds for two sizes of pattern with size randomly varied within a trial sequence or constant throughout a block of trials. This experiment tests the following hypothesis: If internal noise increases with the number of mechanisms monitored and an observer adjusts the number of mechanisms monitored with the size of the stimulus when the size is known, thresholds will be higher in the mixed size condition.

Please cite this article in press as: Foley, J. M. et al., Detection of Gabor patterns of different sizes, ..., *Vision Research* (2006), doi:10.1016/j.visres.2006.09.005

4. Methods

4.1. Apparatus

The stimuli were generated using a computer graphics system that consisted of a PC type computer, a Cambridge Research Systems VSG2/5 graphics board with 15 bits of intensity resolution, and a Clinton monochrome display, model DS2190P with a P45 phosphor operated at a resolution of 1184×848 pixels and a frame rate of 100 Hz. Stimuli were presented using VSG software. Viewed at a distance of 114.7 cm, there were 71.4 pixels/deg and each pixel was 0.84 min on a side. Lookup tables on the graphics board had the dual role of controlling contrast and correcting for the nonlinear relation between voltage and screen intensity. Background luminance was 110 cd/m^2.

4.2. Stimuli

We measured the absolute contrast thresholds of vertical 4 c/deg Gabor patterns of different eccentricities, sizes and shapes. A Gabor pattern is a sinewave grating modulated by a Gaussian window. The spatial luminance functions of our Gabor patterns are described by the equation:

$$L(x,y) = L_0\left[1 + C\exp\left(-\frac{(x-x_s)^2}{2\sigma_{xs}^2} - \frac{(y-y_s)^2}{2\sigma_{ys}^2}\right) \times \sin(2\pi f_s(x-x_s) + \phi_s)\right], \quad (1)$$

where L_0 is the background luminance, C is the contrast parameter, f_s is the spatial frequency, ϕ_s is spatial phase re the pattern center, σ_{xs} and σ_{ys} are the width and height parameters (standard deviations) of the Gaussian envelope, and x_s and y_s are the coordinates of the pattern center re the fixation point. We varied the size and shape of the patterns by varying σ_{xs} and σ_{ys}. Although a Gaussian function does not equal zero at any point, we set its value to 0 for all points more than 3 standard deviations from the center. The temporal waveform was rectangular with a duration of 90 or 240 ms. Appendix A contains a list of all symbols used in this article.

4.3. Procedure

The target contrast threshold was measured with a temporal two-interval forced-choice paradigm. The target was randomly presented in one of the two intervals with equal probability. Tones were presented during the intervals. Other tones provided correctness feedback after each trial. The QUEST procedure Watson and Pelli (1983) was used to adjust the contrast so as to determine the target threshold at the 0.82 probability correct level. The QUEST sequence was terminated after 40 trials, or 50 trials if there were no errors on the last 20 trials. Patterns had rectangular temporal waveforms with different durations used for different observers, 90 and 240 ms. There was a 1 s interval between the two observation intervals. The fixation mark was the intersection of a horizontal and a vertical line, slightly brighter than the background. When the target was centered on fixation, there was a gap in the center. Observers fixated at the center of the gap. The gap increased with the size of the pattern, but was never less than 1 deg or more than 3 deg. There was at least one practice session prior to the start of each experiment and each new spatial phase in Experiment 2. At least six measurements were made in each condition. An outlier test (Rousseeuw, 1991) was used to exclude aberrant measurements. All viewing was binocular with natural pupils. The observers made informal phenomenological reports of the appearance of the target at threshold in the different conditions.

5. Experiment 1: Contrast threshold of a Gabor pattern as a function of its eccentricity

5.1. Method

In this experiment all the Gabor patterns had standard deviations of 0.18 or 0.25 deg (1 wavelength). They were in sine or cosine spatial phase re the center of the pattern. The principal independent variable was their retinal eccentricity. The patterns were always in the center of the screen, and the fixation mark was located along the horizontal line through the center. There were 11 positions of the fixation mark equally spaced within the range of ± 5 deg of the target center. Thresholds at each of these positions were measured in random order. A complete QUEST sequence was run at one position before changing to the next, so there was no objective uncertainty with respect to spatial position. After two practice measurements at each position at least 6 measurements of each threshold were made. There were five observers, two of the authors, JMF and SVR, and three undergraduate students who were naïve with respect to pattern vision research. All had visual acuity of 20/20 or better, with or without correction.

5.2. Results

For all observers log threshold increased as an approximately linear function of eccentricity. Outliers occurred in 4.8% of the measurements and were excluded from the analysis. Standard deviation averaged 1.69 dB over all the data sets. There was a small (15%) increase in standard deviation with eccentricity. Fig. 1 shows the results for the two most consistent observers. The threshold is defined in the conventional way as the value, C_t, of C when the pattern is at threshold. The thresholds are expressed in dB re 1, where $C_{tdB} = 20\log_{10}C_t$. For KRH the function is less steep in the range -1 to $+1$ deg and the straight lines were fitted to measurements outside this range. For both observers thresholds increase more slowly for stimuli to the right of the fixation point than to the left.

Please cite this article in press as: Foley, J. M. et al., Detection of Gabor patterns of different sizes, ..., *Vision Research* (2006), doi:10.1016/j.visres.2006.09.005

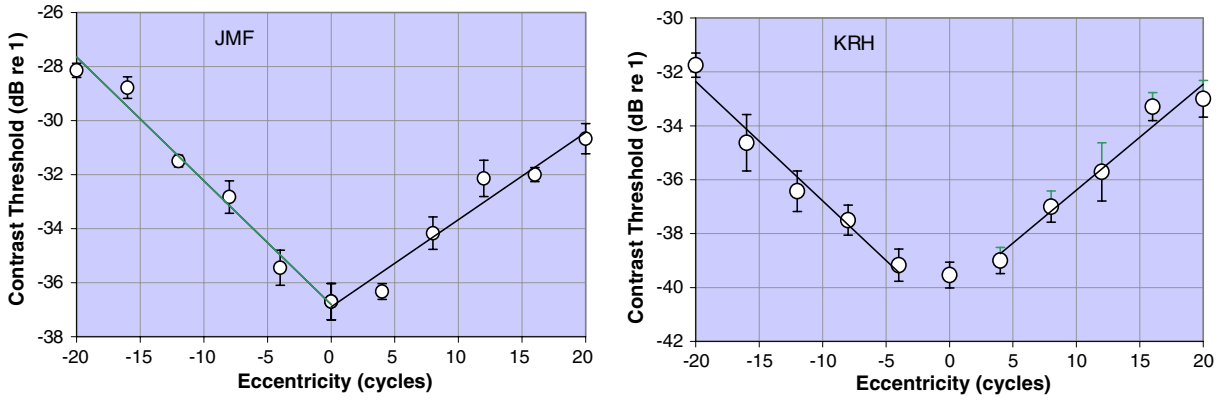

Fig. 1. Contrast threshold of circular Gabor patterns as a function of horizontal eccentricity. Error bars indicate ±1 standard error. Spatial frequency: 4 c/deg, pattern standard deviation: 0.25 deg, spatial phase: 0 deg (sine), duration KRH: 90 ms, JMF: 240 ms.

The linear relation between the threshold in dB and eccentricity implies that the threshold is an exponential function of eccentricity.

$$C_t = C_{t0}\exp(kd), \tag{2}$$

where C_t is the contrast threshold, C_{t0} is the threshold at the fixation point, d is eccentricity, and k is a constant; k will depend on whether eccentricity is measured in degrees or wavelengths. When expressed in dB, threshold is a linear function of eccentricity with slope $20k(\log_{10}e)$. Table 1 gives the slopes and intercepts of the C_{tdB} vs. eccentricity (TvE) plots (for eccentricity in wavelengths). Mean threshold increases approximately 0.47 dB (5.5%) for each one wavelength step in eccentricity. On the right of the fixation point, fits to a straight line are not as good as on the left, and there is more variability in the slopes. These measurements are generally consistent with earlier studies by Robson and Graham and Pointer and Hess cited above. The two most experienced observers produced slightly lower slopes. There is no obvious effect of the two different durations and two different sizes on the slope of the TvE functions. We will use our overall mean slope as a constraint on models of threshold as a function of size.

6. Experiment 2: Contrast threshold as a function of the size and shape of gabor patterns

6.1. Method

Our study is similar in several respects to that of Polat and Tyler (1999). Our targets were vertical Gabor patterns of different sizes and shapes. There were three sets of patterns with respect to shape: (See Fig. 2.):

- Circular patterns: σ_x and σ_y were equal and varied together.
- Collinearly varying patterns: σ_x was constant at 0.25 deg (1 wavelength) and σ_y varied.
- Orthogonally varying patterns: σ_y was constant at 0.25 deg and σ_x varied. (We omit the subscript s in this section because all the symbols refer to the stimulus.)

For each pattern shape set, there were three spatial phases with respect to the center of the pattern, 0 deg (sine), 90 deg (cosine) and 270 deg (anti-cosine). Thresholds were measured as a function of the variable standard deviation of the patterns in each of the nine pattern sets.

The order of the phase conditions was anti-cosine, sine, cosine. All the measurements on one phase were completed

Table 1
Experiment 1: Parameters of the Gabor patterns and the straight lines fitted separately to contrast thresholds to the left and right of the fixation point

Observer	Gabor pattern			Left of fixation				Right of fixation			
	SD (deg)	Phase	Duration (ms)	Slope (dB/cycle)	Intercept (dB re 1)	R^2	k	Slope (dB/cycle)	Intercept (dB re 1)	R^2	k
KC	0.18	Cos	90	−0.47	−32.3	0.91	−0.054	0.47	−32.0	0.79	0.054
KRH	0.25	Sin	90	−0.44	−41.2	0.97	−0.051	0.39	−40.3	0.96	0.045
JMF	0.25	Sin	240	−0.46	−36.8	0.98	−0.053	0.32	−36.9	0.95	0.037
NNS	0.18	Cos	90	−0.50	−32.9	0.93	−0.058	0.49	−32.6	0.86	0.056
SVR	0.18	Cos	90	−0.52	−34.8	0.91	−0.060	0.60	−36.6	0.72	0.069
Mean				−0.48		0.94	−0.055	0.454		0.856	0.052
SD				0.032		0.033	0.004	0.106		0.103	0.012

Please cite this article in press as: Foley, J. M. et al., Detection of Gabor patterns of different sizes, ..., *Vision Research* (2006), doi:10.1016/j.visres.2006.09.005

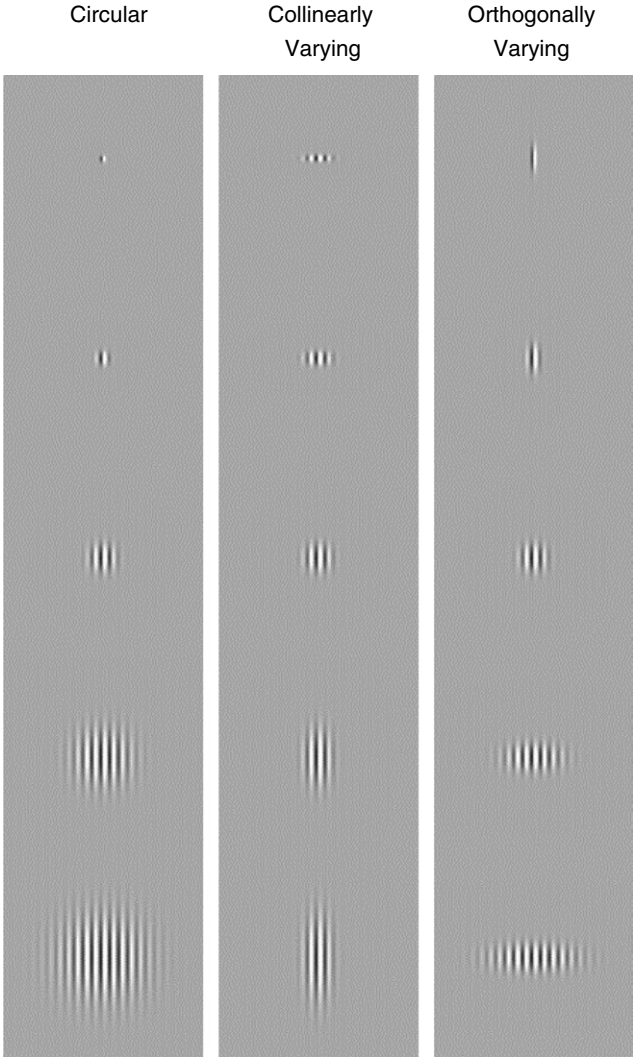

Fig. 2. Examples of patterns used in Experiment 2. The patterns used in Experiments 2 and 3 varied over a wider range than those shown here.

before starting the next. Within each phase condition measurements were blocked by shape and the order of the shapes was counterbalanced over the course of the experiment, except that for anti-cosine and sine phases all the circular pattern thresholds were measured before the elliptical pattern thresholds.

There were two observers, JMF, one of the authors, and HHH, a student, naïve with respect to pattern vision research. Stimulus duration was 240 ms for JMF and 90 ms for HHH. Both had 20/20 visual acuity with correction. Five or more threshold measurements were made for each observer in each condition.

6.2. Results

We define the nominal area of a Gabor pattern as $\pi\sigma_x\sigma_y$ for the purpose of describing our results. Mean thresholds as a function of the variable pattern area for the nine pattern sets are shown in Fig. 3. The standard deviation of the measurements averaged 1.30 dB and the standard error averaged 0.51 dB. Variability was relatively constant across conditions. For each of the pattern sets, the contrast threshold decreases rapidly with pattern size when the patterns are small and more slowly as the patterns get larger. The threshold decreases over our entire range of pattern standard deviations (up to 12 wavelengths). The threshold functions are generally concave upward. For cosine and anti-cosine patterns, threshold decrease is less than proportional to the increase in area. However, for small sine phase patterns that are circular or orthogonal, the threshold decreases by a larger factor than the area increases. For this phase there is a size at which the threshold is inversely proportional to the area of the pattern, but there is no evidence for a range of sizes over which proportionality holds; that would require that the threshold decrease by 20 dB when the area increases by one log unit. For the largest patterns the threshold decreases less than 1/4 log unit (5 dB) for a log unit change in area in most cases. The smooth curves correspond to a model that will be described below.

Circular patterns were found to usually have lower thresholds than elliptical patterns of the same area. An exception occurs for small narrow patterns (orthogonally varying pattern set), which have slightly lower thresholds than circular patterns of the same area. As will be shown in the Models section, this is a consequence of the receptive fields being slightly elongated in the collinear direction.

For small patterns, there is an interaction between shape and size in the determination of thresholds and the direction of the effect depends on pattern phase. In sine phase, thin patterns have higher thresholds than wide patterns of the same area. In cosine and anti-cosine phase, the opposite is true. These effects only occur when the orthogonally varying pattern is very thin. These interactions do not occur for large patterns (σ_x and $\sigma_y \geqslant 0.25$ deg). For large patterns, tall thin patterns have essentially the same thresholds as short wide patterns of the same area. Thus, we do not confirm the main result of Polat and Tyler (1999), even though our experiment was very similar to one of their two experiments in which their 4 c/deg elliptical patterns had a fixed standard deviation of 1 wavelength and a duration of 80 ms.

Although the contrast threshold is the usual measure of detection performance, it is of interest to transform contrast thresholds into contrast energy thresholds. The contrast energy of a pattern is the integral of the square of the contrast function over the pattern, and for vertical Gabor patterns it is given by:

$$\varepsilon = \frac{C^2}{2} T\pi\sigma_x\sigma_y\left[1 - \cos(2\phi)\exp\left(-\frac{4\pi^2\sigma_x^2}{\lambda^2}\right)\right], \quad (3)$$

where T is duration in seconds and the other symbols are the same as in Eq. (1). The derivation of Eq. (3) is given in Appendix B.

As noted above, contrast energy thresholds are of interest because, if the threshold depends on the integral of the product of a receptive field sensitivity function times the

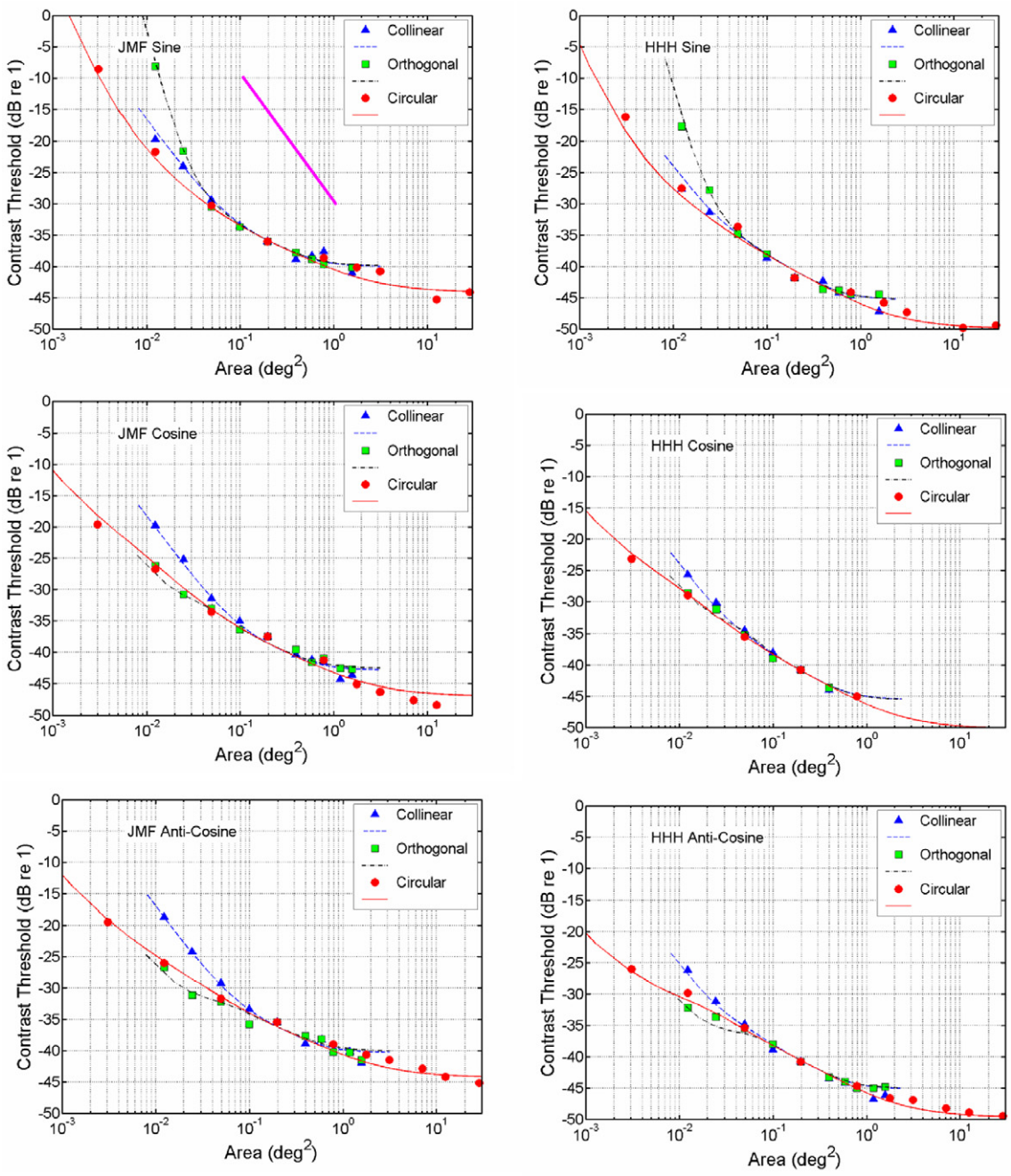

Fig. 3. Experiment 2. Contrast threshold as a function of the area of the Gabor pattern. The figures on the left are for JMF and those on the right for HHH. Each panel shows data for one phase of the pattern re the center of the envelope. The collinear and orthogonal patterns had a fixed standard deviation of 0.25 deg (1 wavelength) in the horizontal and vertical directions, respectively. The smooth curves correspond to a model fitted to the data that is described below. The straight line in the upper left panel has a slope of −20 dB per log unit of area (threshold inversely proportional to area).

contrast function, then contrast energy will be minimum when the receptive field function has the same form as the stimulus pattern and differs from it by at most a scaling factor (Kersten, 1984; Watson et al., 1983). This is a corollary of a well known result in communication theory on matched filter design that states that the most efficient filter or ideal detector for detecting a signal in white noise is one that matches the signal in this sense. Absolute thresholds are limited by internal noise in the visual system. The stimulus with the lowest contrast energy threshold will match the receptive field of the detecting mechanism, only if a single receptive field mediates detection. If a spatial array of receptive fields is involved, as appears to be the case, and receptive field responses are combined nonlinearly, the pattern that produces the lowest energy threshold will not match any one of the receptive fields contributing to detection. As will be shown below, if receptive fields are Gabor-like and their responses are raised to an exponent greater than one and then summed to determine the threshold, at least one of the contributing fields has to have a size smaller

Please cite this article in press as: Foley, J. M. et al., Detection of Gabor patterns of different sizes, ..., *Vision Research* (2006), doi:10.1016/j.visres.2006.09.005

than the single receptive field that would produce the minimum. So energy thresholds can directly provide information about the size of receptive fields, but the relation is not as simple as previous analyses have suggested.

Fig. 4 shows graphs of the contrast energy threshold in deg^2 sec as a function of the variable standard deviation of the pattern. We plot threshold against standard deviation here because it shows the standard deviations at which contrast energy is minimum. Most of the functions have a clear minimum at a standard deviation of 0.12 deg or smaller. Energy thresholds are highest for circular patterns, but that is a consequence of plotting threshold vs. standard deviation. For the same area, thresholds for circular patterns are lowest, except for small orthogonal patterns, as seen in Fig. 3. Here again one sees the same interaction between phase and pattern shape that was apparent in the graphs of contrast threshold vs. standard deviation, so this interaction cannot be entirely explained by differences in the contrast energy of these small patterns. Cosine phase patterns produced slightly lower thresholds than the other two phases, particularly for JMF, but this may be a learning effect since the cosine thresholds were measured last.

In Experiment 3 and the Models section we will show that in many cases more than one receptive field is involved

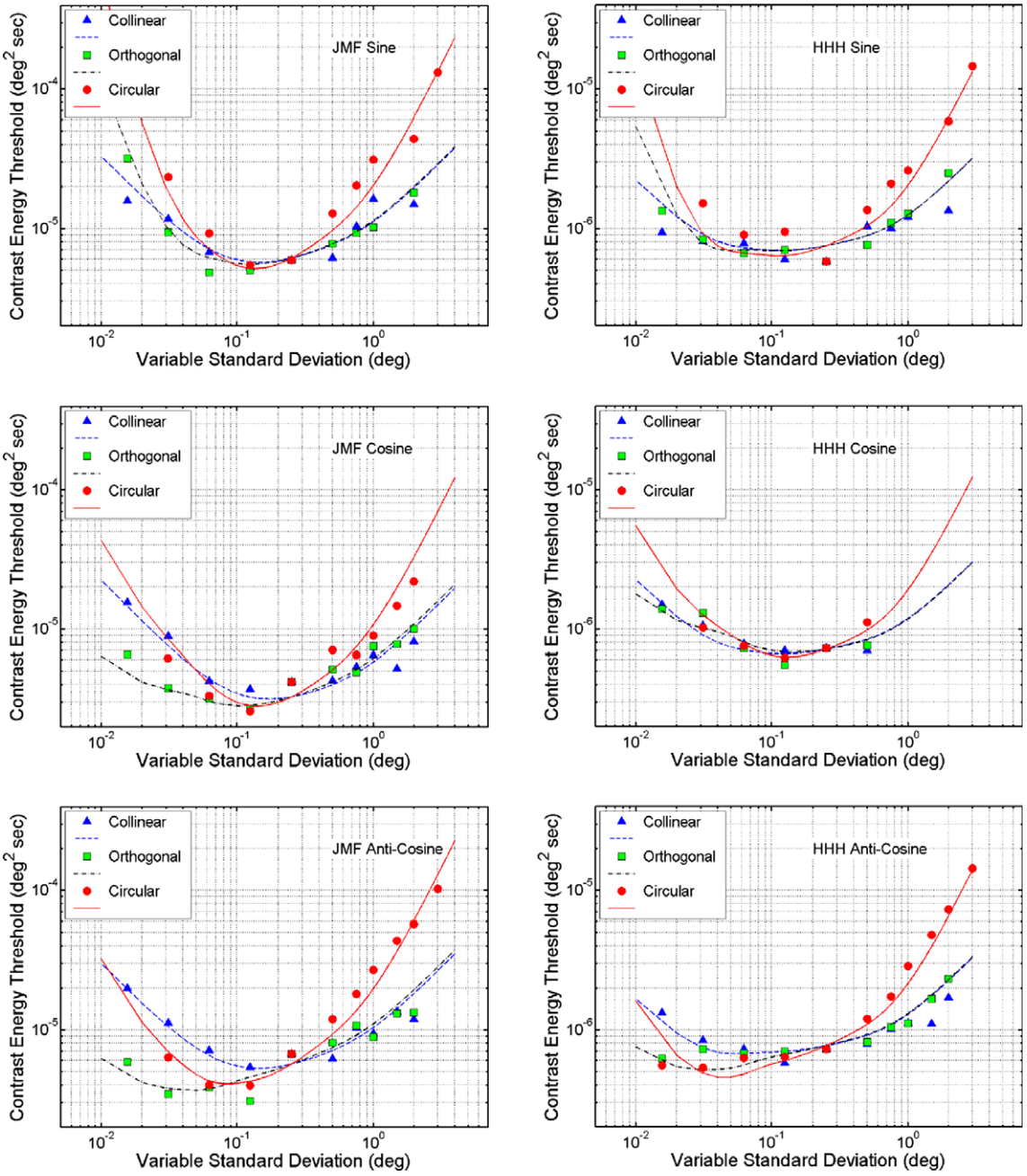

Fig. 4. Experiment 2. Contrast energy threshold as a function of the variable standard deviation of patterns of different shape and phase. The smooth curves correspond to a model that will be described below.

Please cite this article in press as: Foley, J. M. et al., Detection of Gabor patterns of different sizes, ..., *Vision Research* (2006), doi:10.1016/j.visres.2006.09.005

in detecting a pattern, but when this is the case, the minimum of the contrast energy threshold function will occur at a size which is at least as large as the smallest receptive fields. So these energy threshold data indicate that Gabor patterns are detected by receptive fields that are at least this small.

7. Experiment 3: Size discrimination among circular Gabor patterns

Researchers who use phenomenological reports in the study of perceptual systems commonly make the assumption that a single mechanism evokes a single percept that varies in intensity, but not in quality, as the mechanism response varies. This hypothesis can be traced back at least to Johannes Mueller's specific "energies" of nerves and was proposed to apply to single neurons by Helmholtz (Warren & Warren, 1968). This is consistent with the hypothesis that a neuron response has only one information carrying dimension, response rate, which is related to perceived intensity or contrast, and that a single neuron evokes a single percept except for intensity or contrast. This labeled response hypothesis cannot be said to be established, but it has been used by Watson and Robson (1981) to estimate the tuning of detectors for spatial and temporal frequency. It is of interest to ask whether observers can discriminate patterns of different sizes when they are at threshold. A positive result would be consistent with the involvement of more than one mechanism in the detection task. We did an experiment to determine this.

7.1. Method

The patterns were the circular Gabor patterns used in Experiment 2. After measuring their thresholds we set the contrast of each to threshold, the contrast at which responses were 82% correct. Two of these threshold patterns of different sizes were presented on each temporal forced-choice trial. The observer's task was to indicate which of the two patterns was larger. The patterns were selected randomly and presented in random order with the constraint that each pattern was presented the same number of times and equally often in the first and second interval. No feedback was provided. If the set of receptive fields that mediates detection increases with the size of the pattern and the responses of the receptive fields are labeled, for example in position, then we would expect that patterns of different sizes would look different at threshold and be discriminated. Each pattern pair was presented at least 15 times to each observer.

7.2. Results

Fig. 5 presents two different analyses of the results for two observers, JMF and HHH. On the left are graphs of the proportion correct as a function of the number of size

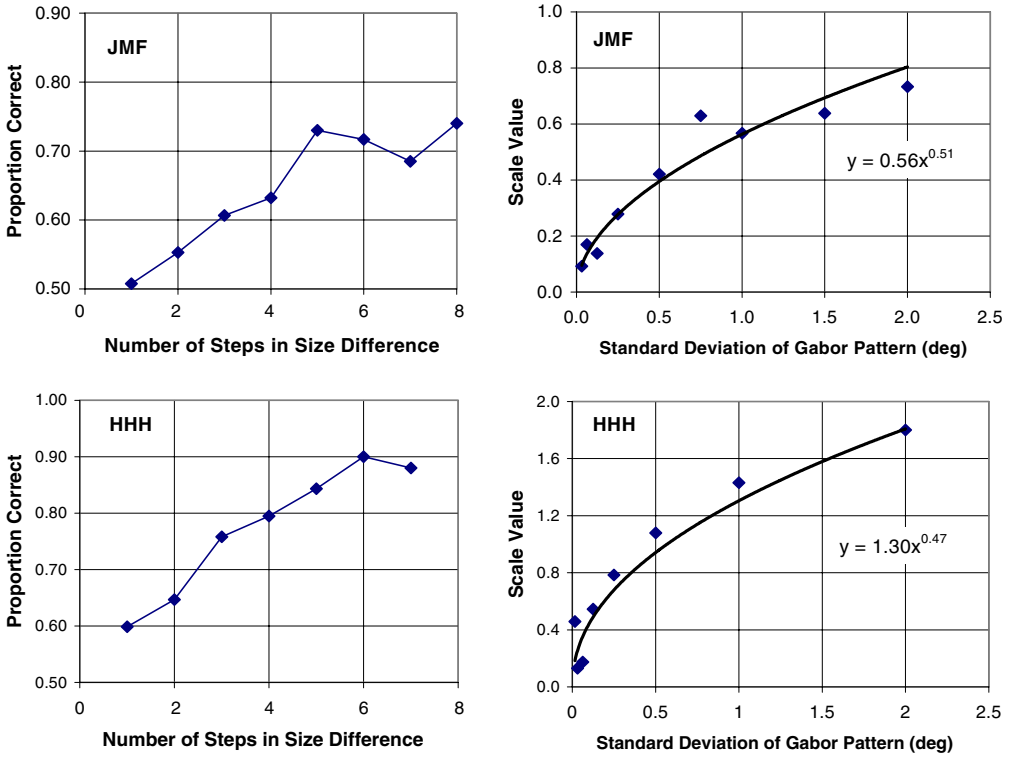

Fig. 5. (Left) Proportion correct as a function of the number of steps in size between patterns. (Right) Thurstone Case V scale of size based on size discrimination results. Since the origin on this scale is arbitrary, a number was added to each scale value so that a 0 scale value would correspond to a 0 size.

Please cite this article in press as: Foley, J. M. et al., Detection of Gabor patterns of different sizes, ..., *Vision Research* (2006), doi:10.1016/j.visres.2006.09.005

steps between the two stimuli. (We use size steps, because all steps do not correspond to the same ratio of sizes. The average step was 1.7 times the standard deviation or 2.9 times the area.) It is clear that both observers can discriminate patterns of different sizes when they are at contrast threshold. Performance improves with the difference between the pattern sizes and appears to reach an asymptote between 70% and 90% correct. One would not expect performance to ever be perfect in this task because at threshold the patterns are not always seen. On the right is a graph of the scale values of the stimuli determined by fitting Thurstone's Case V model to the data (Torgerson, 1958). The difference in scale values between two stimuli indicates how well they are discriminated. The graph shows that discrimination is best among the small patterns and declines as the patterns get larger. For both observers scale value increases as approximately the square-root of standard deviation, although HHH discriminates much better than JMF, as indicated by the larger range of scale values.

7.3. Appearance at threshold

Observers were asked to attend to the appearance of the stimuli at threshold and to describe their appearance. They initially performed a free response task and then were asked questions to clarify the appearance of the patterns. The smallest patterns evoked percepts that were described as one, two, or three short vertical stripes. Often only a single stripe was seen and it was more often dark than bright. Larger patterns evoked percepts of grating patches. These were much smaller than the stimuli, but usually several adjacent stripes were seen. The overall shape varied from trial to trial and was sometimes irregular. A common shape was ellipse-like with the long axis horizontal. The percept was often not centered on the fixation point. The patch was usually one continuous region of roughly uniform perceived contrast except at the edges where contrast faded. These reports are consistent with the hypothesis that detection of the larger patterns is mediated by an array of receptive fields each of which evokes a local percept. The fact that the percepts are almost always continuous patches suggests that interpolation in the visual system may contribute to filling in the percept.

8. Experiment 4: Effect on thresholds of mixing pattern sizes within blocks of trials

In many experiments it makes a difference whether or not an observer knows what stimulus will be presented on a given trial. Thresholds are lower when an observer has this knowledge. This result is usually explained by models in which the observer can take advantage of this knowledge by basing the decision only on signals from mechanisms that are sensitive to the known stimulus. See, for example, Foley and Schwarz (1998). The model assumes that, if the observer combines signals from mechanisms that are insensitive to the stimulus and signals from sensitive mechanisms that the variance of the decision variable will be greater than when only signals from sensitive mechanisms are combined, and consequently a higher contrast will be required at threshold.

The results of Experiment 3 suggest that there is a spatial array of mechanisms in the region of the retina where the patterns are imaged. The subset of mechanisms that are sensitive to a pattern increases with pattern size. If the observer bases his or her decision on the responses of increasing numbers of mechanisms as pattern size increases, and the variance of the decision variable increases with the number of mechanism responses that are combined, then we would expect that thresholds would be higher in conditions in which different sizes are randomly intermixed within a block of trials. Specific predictions depend on the observer's strategy in the mixed condition. If the observer always combines responses from the set of mechanisms sensitive to the larger pattern, then the threshold for the smaller pattern will increase. If the observer combines responses from the set of mechanisms sensitive to the smaller pattern, the threshold for the larger pattern will increase. With any other strategy, both thresholds will increase.

We did an experiment to determine the effect of presenting different sizes in random order within a single block of trials. The patterns were circular Gabor patterns with standard deviations of 0.063 and 1 deg (ratio of areas: 1:255). The method was the same as in Experiment 2 except that in each condition there were two Quest sequences that were interleaved randomly. The pattern size in the two sequences was either the same (blocked sizes) or different (mixed sizes). There were two observers JMF, who participated in all the experiments and VHN, who participated only in this one. For JMF the patterns were in cosine phase with a duration of 240 ms and there were 8 measurements in each condition; for VHN patterns were sine phase with a duration of 90 ms and there were 12 measurements in each condition. The results are given in Table 2. There are very small and inconsistent differences between the Blocked and Mixed conditions, none of which approach statistical significance. Meese, Hess, and Williams (2005, Expt. 2) reported a similar study in which there were four pattern sizes presented in either blocked or mixed sequences. They found essentially a very small effect in favor of the blocked trials (<.25 dB) for two subjects and no effect for the third.

9. Models

We examined a large number of models that are similar, but differ in some respects. The models are elaborations of the model proposed by Foley (1994) and Foley and Chen (1999). According to these models, detection is mediated by one or more mechanisms that are characterized by a receptive field that sums contrast linearly followed by a nonlinear transformation from this sum to the response of the mechanism. Here the original model is elaborated

Please cite this article in press as: Foley, J. M. et al., Detection of Gabor patterns of different sizes, ..., *Vision Research* (2006), doi:10.1016/j.visres.2006.09.005

Table 2
Experiment 4: Contrast thresholds for two sizes of Gabor patterns in blocked and mixed experimental designs

Observer	Blocked sizes – Pattern SD (deg)		Mixed sizes – Pattern SD (deg)		Blocked–Mixed – Pattern SD (deg)		Probability of t under null hypothesis	
	0.0625	1	0.0625	1	0.0625	1	0.0625	1
JMF	−27.75	−48.25	−28.00	−47.63	0.25	−0.63	>0.25	>0.25
VHN	−31.33	−48.50	−30.50	−48.83	−0.83	0.33	>0.10	>0.25
Mean	−29.54	−48.38	−29.25	−48.23	−0.29	−0.15		

by specifying the form of the receptive field sensitivity functions (Gabor functions) and estimating their parameters.

Two-dimensional Gabor functions have often been used to represent the spatial receptive fields of visual neurons in V1 and V2 (Marcelja, 1980; Ringach, 2002). When the sensitivity modulation is in the horizontal direction and the envelope is symmetrical about the x and y axes this function is given by the following equation:

$$s(x,y) = S\exp\left[-\frac{(x-x_f)^2}{2\sigma_{xf}^2} - \frac{(y-y_f)^2}{2\sigma_{yf}^2}\right]\sin(2\pi f_f(x - x_f) + \phi_f), \quad (4)$$

where S is a sensitivity parameter, x_f, y_f, are the coordinates of the center of the receptive field, σ_{xf} and σ_{yf} are the standard deviations of the field in the horizontal and vertical directions, respectively, f_f is the spatial frequency of the receptive field, and ϕ_f is the phase of the sinewave re the center of the receptive field. To account for our data we found that we needed a spatial array of receptive fields of this form.

According to the model, detection is mediated by one or more mechanisms that are characterized by a receptive field that sums contrast linearly followed by a nonlinear transformation to a response. The mechanism responses are summed to compute a detection variable that determines the threshold. Here we are concerned only with the absolute threshold of patterns in the absence of context patterns. We assume that near absolute threshold divisive inhibition is sufficiently small that it can be ignored.

In this study our patterns are vertical Gabor patterns. We assume that their detection is mediated by linear vertical Gabor receptive fields. Foley and Chen (1999) showed that receptive fields having four phases re the fixation point (0, 90, 180, and 270 deg) are sufficient to account for phase effects in masking. We assume the same four phase types.

We define the excitation E_{ij} of specific receptive field j produced by specific pattern i as:

$$E_{ij} = \int_{-\infty}^{\infty} dy \int_{-\infty}^{\infty} dx c_i(x,y) s_j(x,y). \quad (5)$$

In Appendix C we derive an equation for E_{ij}. The expression for E_{ij} may be expressed as:

$$E_{ij} = C_i S_j F_{ij}, \quad (6)$$

where C_i is the contrast parameter of the pattern, S_j, is the sensitivity parameter of the receptive field (S in Eq. (4)), and F_{ij} is a factor that depends on both the pattern and the receptive field. (See Appendix C, Eq. (C17), (C18).) Based on our measurements and others in the literature, we assume that the sensitivity parameter of the receptive fields decreases as an exponential function of the eccentricity, d_j, thus:

$$S_j = S_0 a^{d_j}, \quad (7)$$

where S_0 is the sensitivity factor for a receptive field centered on the pattern and $a = e^{-k}$ is an eccentricity parameter, the factor ($a < 1$) by which sensitivity decreases for each wavelength increase in eccentricity. If we define the sensitivity of receptive field j to pattern i, s_{ij}, as:

$$s_{ij} = S_0 a^{dj} F_{ij}, \quad \text{then}: \; E_{ij} = C_i s_{ij}. \quad (8)$$

We assume that negative excitation does not produce a response, and therefore we define effective sensitivity, s'_{ij}, and effective excitation, E'_{ij}, as:

$$s'_{ij} = \max(0, s_{ij}) \text{ and } E'_{ij} = C_i s'_{ij}. \quad (9)$$

The response of a mechanism when contrast is near threshold is:

$$R_j = (E'_{ij})^m. \quad (10)$$

The detection variable for the pattern i, D_i, is the sum of the responses over the mechanisms:

$$D_i = \sum_{j=1}^{n} R_j = \sum_{j=1}^{n} (C_i s'_{ij})^m = C_i^m \left[\sum_{j=1}^{n} (s'_{ij})^m\right]. \quad (11)$$

At threshold, $D_i = 1$ and the contrast threshold C_t is:

$$C_t = \left(\sum_{j=1}^{n} (s'_{ij})^m\right)^{-1/m}. \quad (12)$$

Given this general model, we fitted a large number of specific versions of it to our data.

It is important to distinguish among the several different "sensitivities" referred to in this paper. An observer's sensitivity to a stimulus is the reciprocal of the observer's threshold for that stimulus. In the model we distinguish between the sensitivity function of a receptive field $s(x,y)$, the sensitivity parameter of that receptive field, S, and the sensitivity of a receptive field j to a particular pattern i, s_{ij}, which is the reciprocal of the threshold of that receptive field to the pattern, and s'_{ij}, which is the effective sensitivity of j to i.

When we sum responses over receptive fields to form a detection variable, we assume that the information about the individual receptive field responses and their position labels is not lost. If it were lost, observers would be unable to discriminate size at absolute threshold. These responses determine the percept and are the basis for the size discrimination shown in Experiment 3.

Each version of the model assumes a regular array of one or more vertical Gabor receptive fields. The center field is centered on the fixation point and the other fields are separated from it horizontally at intervals of 2, 1, and 0.5 wavelengths. This implies that for the intervals of 2 and 1 wavelengths, only the fields having the same phase as the pattern will be excited and, for the interval of 0.5 wavelengths, only the fields in phase and half a wavelength out of phase will be excited. All the receptive fields in each array were tuned to the same spatial frequency and had the same standard deviations. They differed in position, and their sensitivity, S, decreased as an exponential function of eccentricity in wavelengths. The sensitivity parameter of the center receptive field, S_0, the standard deviations of the receptive fields, σ_{xf} and σ_{yf}, and the response exponent, m were free parameters in most fits. In some fits the center frequency, f_f, the phase, ϕ_f, or the eccentricity factor, a, were free parameters.

When the receptive field center frequency and phase were free parameters, estimates of both parameters varied, although 5/6 of the spatial frequency estimates were between 3.97 and 4.01, close to the spatial frequency of the patterns (4 c/deg). Goodness of fit was little improved by allowing these parameters to be free and in some cases there were several fits with different parameters that were about equally good. Consequently, we fixed the spatial frequency parameter to 4 c/deg and the phases to be 0, 90, 180 and 270 deg. Likewise, when the eccentricity parameter, a, was a free variable, estimates varied with data set. Since we have an independent estimate of this value from Experiment 1, we fixed a at that value ($a = 0.947$). When we restricted the number of parameters there was usually one clearly best fit. The principal parameters that we explored were the size and shape of the receptive fields, their number and layout, and the exponent to which receptive field excitation was raised to give the response of the mechanism. For each array of receptive fields we compared models with circular and elliptical receptive fields. For some of our models these best fits are very good with little systematic error. Thus, relatively simple models describe performance well. They are undoubtedly simpler than the visual system.

We started with a model having a single receptive field centered on the pattern. We compared this with models in which the receptive fields were laid out in square lattices containing 25, 49, and 169 receptive fields. For each of these arrays the outermost receptive field centers lay on a square 6 wavelengths on a side centered on the pattern. The spacing between receptive field centers was 2, 1, and 0.5 wavelengths, respectively. We also fitted a model with a hexagonal array of receptive field centers. This had 1 wavelength spacing horizontally and 1.15 wavelength spacing vertically and the outermost receptive field centers lay on a hexagon 6 wavelengths wide and 6.92 wavelengths high.

The data allow us (i) to test the hypothesis that the patterns are detected by receptive fields whose sensitivity functions are two-dimensional Gabor functions, (ii) to estimate the parameters of those receptive fields, and (iii) to examine the effects of different arrays of receptive fields. Each of the six data sets from one observer and one pattern phase was fitted separately. Data for all three pattern sets, circular, collinearly varying, and orthogonally varying, were fitted together using a single array of receptive fields. The criterion of least root mean squared error (RMSE) was used to determine the best fit. Our fitting routine first performed an array search over a large array of possible parameter values, decreasing the ranges of the values on each pass until a criterion of failure to improve was met. It then took the best values from array search as input to a minimization routine based on the MATLAB function fminsearch. To compare nested models we used F-tests (Khuri & Cornell, 1987) to determine if the improvement in goodness of fit obtained by allowing the receptive field to be elliptical or allowing the spatial summation parameter, m, to vary over data sets was statistically significant. Only nested models can be compared by this test. Table 3 summarizes some of the models and gives the parameters of best fit.

9.1. Single receptive field models

We first fitted a single Gabor receptive field (RF) model to each of the six data sets. We varied the sensitivity of this field and its standard deviations to find the best fit. The RMSE of the best circular Gabor model was 1.86 dB and that of the best elliptical Gabor model was 1.78 dB. Although the fit is not extremely bad, in every case there is the same systematic error. Predicted thresholds are too high for small and large patterns and too low for middle-sized patterns, and the predicted function is more curved than the empirical one.

We then asked if a single receptive field model would fit the data for the small patterns. We restricted the fit to patterns with a variable standard deviation less than or equal to 0.125 deg (0.5 wavelength). In this case the fits were substantially better with average RMSE equal 1.30 for the circular RF and 1.04 for the elliptical RF. The RF's providing the best fit are very small with average $\sigma = 0.10$ deg for the circular RF and $\sigma_x = 0.09$ deg and $\sigma_y = 0.11$ deg for the elliptical RF. However, this model is clearly inadequate for large patterns; it predicts thresholds that are far too high. For two of the six data sets (JMF, cosine and anti-cosine phase), an elliptical receptive field about 1.5 times longer in the collinear direction than the orthogonal direction gave significantly better fit than the circular model. In the other four cases the elliptical model was not significantly better than the circular one.

Please cite this article in press as: Foley, J. M. et al., Detection of Gabor patterns of different sizes, ..., *Vision Research* (2006), doi:10.1016/j.visres.2006.09.005

Table 3
Comparison of Model Fits

Model	Single RF	Single RF	Square 25[a]	Square 49	Square 169	Square 169	
		Small patterns	$m = 2.9$	$m = 2.9$	$m = 2.9$	$m = 2.49$	$m = 3.08$
Number RF's	1	1	25	49	169	169	
Layout			Square	Square	Square	Square	
Spacing of RF's (wl.)			2	1	0.5	0.5	
Size of array (wl.)	0	0	6×6	6×6	6×6	6×6	
Parameter values and RMSE						HHH only	JMF only
Circular RF Model							
S_0	2210	3405	3147	3282	3646	5838	2144
σ (deg)	0.157	0.101	0.102	0.089	0.067	0.051	0.077
m	1	1	2.9	2.9	2.9	2.49	3.08
RMSE	1.86	1.30	1.14	1.05	0.99	0.87	1.04
Elliptical RF Model							
S_0	2232	3449	3160	3303	3695	6070	2085
σ_x (deg)	0.136	0.092	0.093	0.082	0.060	0.048	0.065
σ_y(deg)	0.186	0.111	0.112	0.097	0.075	0.053	0.095
m	1	1	2.9	2.9	2.9	2.49	3.08
Ratio: σ_y/σ_x	1.37	1.20	1.20	1.19	1.25	1.09	1.47
RMSE	1.78	1.04	1.04	0.95	0.89	0.81	0.89

In this table the subscript f is omitted because all standard deviations are for receptive fields.

[a] In this model alternate rows and columns of RF centers were offset by one wavelength. Within each row and column centers were separated by 2 wavelengths.

9.2. Multiple receptive field models

At this point we could have looked for an alternative to the Gabor sensitivity function. However, the facts that the Gabor model fits thresholds for small patterns very well and the percept of a Gabor pattern at threshold increases in perceived size with the size of the pattern suggest that more than one receptive field mediates the detection of large patterns. Consequently, we examined models in which an array of mechanisms with Gabor receptive fields mediates detection. We determined the value of the nonlinear response parameter, m, by making it a free parameter (in addition to the sensitivity parameter and standard deviations) and then taking the mean over all data sets ($m = 2.9$) or the three data sets for each observer ($m = 2.49$, 3.08). We then fixed m at these values and used our model fitting routine to determine the best values of the other parameters. The smooth curves in Figs. 2 and 3 correspond to the predictions of the best such model that we found. This model is described in the two rightmost columns of Table 2. This model has 169 receptive fields arranged in a square array with half wavelength spacing in the horizontal and vertical directions. The best fields are elliptical with σ_y greater than σ_x. Mean RMSE is 0.89 dB for JMF and 0.81 for HHH. Fig. 3 shows that the model fits well with little systematic error. Thus, an array of receptive fields all of the same size and shape can mediate detection of patterns with a wide range of sizes and shapes.

We fitted several other models that differed in the number of receptive fields and their layout. Table 3 summarizes a few of these models. The number of receptive fields varied from 25 to 169. Most were square arrays, but one was hexagonal. All of these models fit the data well, but goodness of fit increases slowly with the density of the receptive fields. For small arrays the best receptive field standard deviations are about 0.1 deg, but they become progressively smaller as the density of receptive fields increases, averaging about 0.065 deg when the spacing is half a wavelength. Since the differences in RMSE among these models are not great, we are left with some uncertainty about the tradeoff between receptive field size and density. However, it is clear that the best receptive fields have standard deviations in the range of 0.05–0.1 deg (0.2–0.4 wavelengths).

For every data set and every model, an elliptic receptive field fitted the data better than the circular field. The best receptive field was almost always longer in the vertical (collinear) direction. However, for 4 out of 6 data sets the improvement in fit of the elliptic model over the circular model was not statistically significant. The exceptions were JMF cosine and anti-cosine. For the best model (smooth curves in Figs. 2 and 3), mean σ_y/σ_x was 1.47 for JMF and 1.09 for HHH. We conclude that at least in some cases the best receptive field shape is elliptical with the long axis collinear with the stripes.

When the response parameter, m, is free to vary, best values are found between 2.3 and 4.2 for the different data sets. The average value across data sets and observers is about 2.9 and it varies very little across models. The goodness of fit is not very sensitive to the value of m. This is shown by the fact that allowing m to be a free parameter that varies with data set almost never produces a significant improvement in fit over the case where $m = 2.9$. So we cannot be confident about the values of m. However, when we fitted the 169 receptive field model with the exponent constrained to be 1, for every data set the RMSE was much

Please cite this article in press as: Foley, J. M. et al., Detection of Gabor patterns of different sizes, ..., *Vision Research* (2006), doi:10.1016/j.visres.2006.09.005

higher and this difference is statistically significant with $P < 0.001$. So the data are not consistent with linear summation across receptive fields. Our values for m are lower than those found in some studies, but they are consistent with the values determined from psychometric functions by Foley and Legge (1981), including those of one of our observers, JMF, and they are also consistent with values estimated from several different models of the ModelFest data (Watson & Ahumada, 2005). Our hexagonal array model had 37 receptive fields and produced a RMSE between the RMSE's for square arrays of 25 and 49 receptive fields. Thus, the data do not appear to discriminate between square and hexagonal arrays.

It is of interest to examine the effects of the different parts of the receptive field array on the system threshold. We have done that by computing the contrast thresholds and contrast energy thresholds separately for the center receptive field and those of successive squares of receptive fields going out from the center. Graphs showing the thresholds for these subsets of receptive fields and for the entire set are shown in Fig. 6.

The top graphs are for a square array of 49 receptive fields with 1 wavelength spacing. They show that patterns with standard deviations less than 0.1 deg are detected by a single mechanism and that the minimum in the energy threshold function occurs at this standard deviation. The bottom graphs are for an array of 169 receptive fields with 0.5 wavelength spacing. In this case for patterns with standard deviations greater than 0.05 deg, both the center mechanism and the innermost square of mechanisms contribute to detection. The minimum in the energy function is between the minima for the center receptive field and the minimum for the inner square alone. This illustrates why it is that, when the array is dense, the receptive fields estimated from the model fit must be smaller than the pattern at the minimum of the energy function.

9.3. Explanation of the shape by size interaction

It is apparent in Figs. 3 and 4 that for small patterns there is an interaction between shape and size that depends on phase. These interactions are completely accounted for by the model. To understand these interactions, consider what happens when a narrow vertical Gabor pattern becomes increasingly narrow. If the pattern is in sine phase, its peak amplitude and contrast energy decrease rapidly. On the other hand, for a pattern of constant width that becomes increasingly short, the peak amplitude remains constant and contrast energy decreases slowly. However, this stimulus difference is not the entire explanation, since

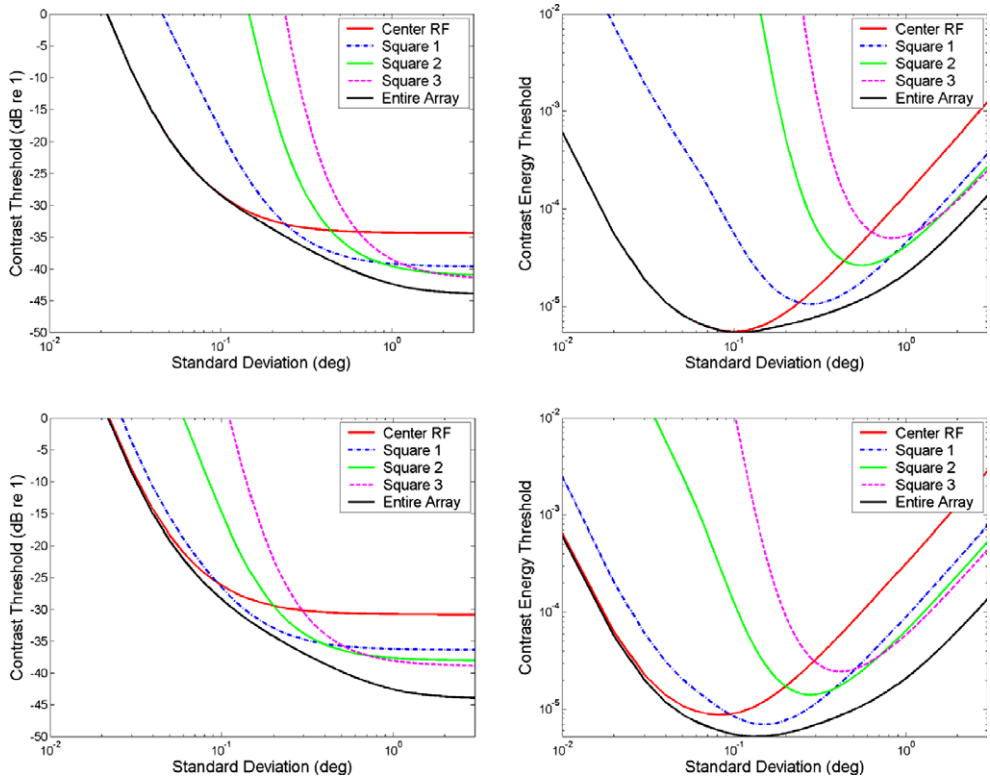

Fig. 6. (Top) 49 receptive fields, spaced 1 wavelength center to center. Threshold for the center receptive field alone and each of the squares of receptive fields going out from the center. Parameters are the best fitting values for JMF circular RF, sine phase, $S_0 = 2072$, $\sigma_x = 0.094$, $\sigma_y = 0.094$, $m = 2.9$. The graphs show that for this model the center receptive field alone mediates detection of patterns with standard deviations less than 0.1 deg (0.4 wavelengths). (Bottom) 169 receptive fields, spaced at 0.5 wavelengths. Parameters are the best fitting values for JMF sine phase, $S_0 = 70$, $\sigma_x = 0.078$, $\sigma_y = 0.078$, $m = 2.9$. In this model the first square contributes to the detection of the most visible pattern and the minimum in the function occurs at a standard deviation larger than that of the smallest receptive field.

Please cite this article in press as: Foley, J. M. et al., Detection of Gabor patterns of different sizes, ..., *Vision Research* (2006), doi:10.1016/j.visres.2006.09.005

the energy thresholds also show the interaction. As the two patterns get smaller, the sensitivity of the regions of the sine phase receptive field that underlie the pattern also change in a similar way resulting in a further increase in the threshold difference. In addition, the elliptical shape of the receptive fields affects the sensitivity of the regions underlying the two patterns and influences the magnitude of the interaction. When the pattern and the receptive field are of cosine or anti-cosine phase, the effects are opposite to those for sine phase. As the thin cosine or anti-cosine pattern gets thinner, its peak amplitude does not change at all and its contrast energy changes slowly, more slowly than that of a pattern of the same area that is getting shorter. Likewise, the same relative changes occur in the sensitivity of the regions of the receptive field underlying these patterns.

9.4. Other models

We have shown that a model in which the receptive field sensitivity is a two-dimensional Gabor function of space and there is an array of receptive fields, identical except for an exponential decrease in sensitivity with eccentricity and arranged in a square lattice, gives a good account of these data. The model assumes that the spatial frequency and spatial phase of the receptive fields matches that of the stimuli. However, it is unrealistic to expect that there is a receptive field matching every spatial frequency and phase. We explored the effect of a mismatch by making fits with frequency constrained to values between 3.5 and 4.5 c/deg in the 169 receptive field model. Within this range a frequency mismatch had very little effect on goodness of fit.

We further explored the effects of mismatches using a program that simulated the 169 receptive field model. The sensitivity of a frequency mismatched receptive field depends on its size, shape, and sensitivity parameter as well as its frequency and phase. If its standard deviation is inversely proportional to its spatial frequency and its sensitivity parameter is the same as the best field, small mismatches in frequency or phase do not affect the form of the TvS function for individual receptive fields. For patterns with standard deviations less than 0.1 deg, effects of small mismatches in frequency are negligibly small. For larger patterns receptive fields tuned to higher frequencies have higher thresholds. Receptive fields tuned to lower frequencies may have lower thresholds due to their larger size, so it is possible that patterns of different sizes could be detected by receptive fields tuned to different frequencies. The effect of a phase mismatch is to increase thresholds for all pattern sizes. A mismatch of 0.3 radians increases thresholds by about 1 dB. So our results are insufficient to determine the spatial frequency or phase of the detecting receptive fields, except that they cannot be greatly different from those of the patterns. Further, we cannot rule out the possibility that more than one type of receptive field mediates performance for a single pattern. We have simulated cases in which there are three types of receptive fields that differ in spatial frequency and/or phase. If they are all similar to the pattern, they will be sensitive to it and have the effect of decreasing the threshold below that for a single mechanism type. The TvS function for a set of receptive fields that are similar to the matched receptive field will be similar in form to that of the single matched field.

The model presented above is a deterministic model. It does not account for the fact that responses to a constant stimulus vary randomly from trial to trial or take into account the noise in the visual system that manifests itself in many experiments. As such it belongs to a large set of deterministic models that describe some phenomena well, but not all.

There are a large number of multiple mechanism, internal-noise-limited detection models that vary in the probability distributions of the noise and the nature of the detection process. Graham (1989) analyzes many of these models. One of these is Quick's high threshold pooling model (Quick, 1974), which assumes that each mechanism either detects or does not detect the pattern on every trial. Although the model is probabilistic, the equations can be interpreted deterministically to predict thresholds without making all the assumptions. The rule for combining responses across mechanisms is very similar to Eq. (11), except that Quick raises the sum of responses to the $1/m$ power. In our case this power has no effect since the sum is equal to 1 at threshold. Without the $1/m$ power, the model implies that the excitations of the receptive fields are raised to a power and then summed linearly to yield the detection variable. Quick's model describes a lot of results fairly well, but fails in critical tests (Graham, 1989). We note the formal similarity of our predictions to those made by the Quick model. Although we sum the nonlinear mechanism responses linearly, the data do not require this. Since, at threshold, the left side of Eq. (11) is 1, the right side could be raised to any power and it would still equal 1. Thus, the Quick model can account for our threshold data. However, it is not the only model that can do this.

There are many models that assume that the mechanisms can produce a range of response values. Some make optimal use of the signals available; others do not. To date there is no clear best model of pattern detection. The most commonly assumed probability distributions are Gaussian and there is evidence that variance increases with mean response (Kontsevich, Chen, & Tyler, 2002). Decision rules are usually based either on sums of responses across mechanisms or maxima of responses across mechanisms. Models differ in whether only responses of mechanisms that are sensitive to the stimulus are taken into account or the decision is based on responses of a larger set of mechanisms possibly as a consequence of objective and/or subjective uncertainty as to which mechanisms are sensitive to the particular stimulus being presented.

According to signal detection theory (Green & Swets, 1966) the threshold for any stimulus, i, depends on a decision variable that varies randomly from trial to trial. In the absolute threshold case, the threshold depends on the ratio, d', of the mean response, to the standard deviation of the

Please cite this article in press as: Foley, J. M. et al., Detection of Gabor patterns of different sizes, ..., *Vision Research* (2006), doi:10.1016/j.visres.2006.09.005

responses, σ_i. To create a signal detection model of our data, we assume that the mean response equals D_i. Then:

$$d'_i = \frac{D_i}{\sigma_i} = \frac{1}{\sigma_i}\left(C_i^m\left[\sum_{j=1}^{n}(s'_{ij})^m\right]\right). \quad (13)$$

At threshold we assume that $d'_i = 1$, which implies that:

$$\sigma_i = C_i^m\left[\sum_{j=1}^{n}(s'_{ij})^m\right]. \quad (14)$$

Thus, in this model there is a trade-off between the value of m and the function σ_i that relates the standard deviation of the decision variable to the parameters of the pattern. The deterministic model is equivalent to the signal detection model with m equal to a fixed value (2.49 or 3.08 for our two observers) and σ_i equal to 1. Any other value of m requires that σ_i vary with the size and shape of the pattern. In Fig. 7, we plot the function $\sigma(A_i)$ for the case of JMF and circular patterns. It can be seen that when $m < 3.08$, $\sigma(A_i)$ increases with area and asymptotes for areas greater than 1 deg^2. If $m > 3.08$ standard deviation must decrease as area increases. A decrease does not seem plausible.

So, although it is likely that the responses are perturbed by noise, our data do not determine whether this noise is constant over different sizes of patterns or increases with the size of the pattern. What might cause the standard deviation to vary with the size of the pattern? One hypothesis is that, since the trials are blocked by pattern size, the observer takes advantage of that information and sums responses over only a subset of the array of receptive fields, a subset of fields that are most sensitive to the pattern. If the noise is independent across fields, the variance of this sum will be the sum of the variances of the summed responses and will increase with the number of fields that contribute to this sum. If this were the case, we would expect that if patterns of different sizes were presented in random order within blocks of trials, performance would be worse. An alternative model in which the observer's decision is based on the maximum response taken over a set of mechanisms that varies with pattern size, makes this same prediction (Tyler & Chen, 2000).

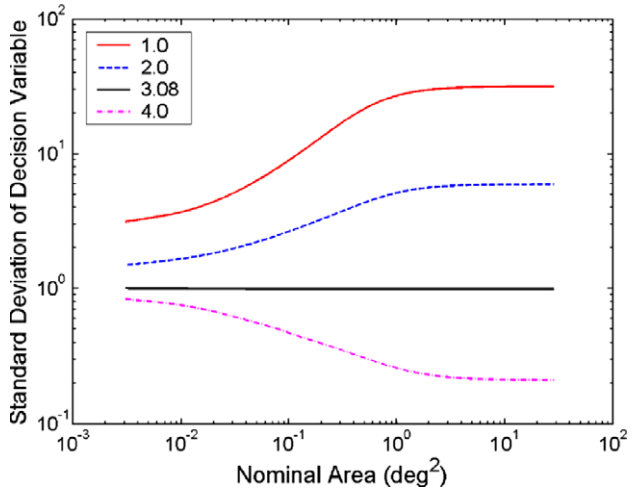

Fig. 7. Signal detection model. Trade-off between the value of m and the function relating the standard deviation of the decision variable to the area of the pattern (based on the data of JMF, sine phase, circular patterns). The value of m estimated from the deterministic model is 3.08. This corresponds to the signal detection model with decision variable standard deviation constant and equal to 1.

Experiment 4 tested this hypothesis and rejected it. This result implies that either the number of mechanisms whose responses are combined does not vary with stimulus size, or the standard deviation of the decision variable does not vary with the number of mechanisms whose responses are combined, or both. Since there is evidence that in other conditions the number of mechanisms whose responses are combined varies, the latter seems to be the more likely.

10. Discussion

Although the general form of our threshold vs. size functions is similar to others in the literature, ours are consistent in showing that the general form of the relation between contrast threshold and size is concave up on log–log coordinates. Although segments of these functions can be fitted with straight lines with a wide range of negative slopes, we think that the smooth curves predicted by the single Gabor receptive field model provide the best account of thresholds for small patterns. The hypothesis that templates are available to match each pattern or a range of patterns is not excluded by the data, but it requires that this set of templates has the same sensitivity to each pattern as our single receptive field. This is not a parsimonious model. For large patterns, it is clear that some kind of nonlinear summation over RF excitations is operating. We have described one model of this summation, but we cannot exclude other models.

Our data are well fitted by a model in which there is an array of receptive fields whose sensitivity functions are two-dimensional Gabor functions. The fields are identical, except for a sensitivity parameter that decreases exponentially with eccentricity. These fields have standard deviations of 0.2–0.4 wavelengths at 4 c/deg, and the standard deviation is on average 30% longer in the direction collinear to the stripes. Fig. 8 shows cross-sections of the sensitivity functions for receptive fields of these sizes. Since goodness of fit varies little between these two models, we are left with this range of possible receptive field densities and associated receptive field sizes.

When the standard deviation is reduced from 0.4 to 0.2 wavelengths, the two outer lobes almost disappear, greatly increasing the bandwidth. A standard deviation of 0.2 wavelengths is very small. It is almost a small blob detector and has a very broad bandwidth. This is inconsistent with other results and may indicate that the receptive field spacing is more than 1/2 wavelength. On the other hand, the ModelFest stimulus with the lowest contrast energy threshold was a small Gaussian blob (Watson & Ahumada, 2005).

Please cite this article in press as: Foley, J. M. et al., Detection of Gabor patterns of different sizes, ..., *Vision Research* (2006), doi:10.1016/j.visres.2006.09.005

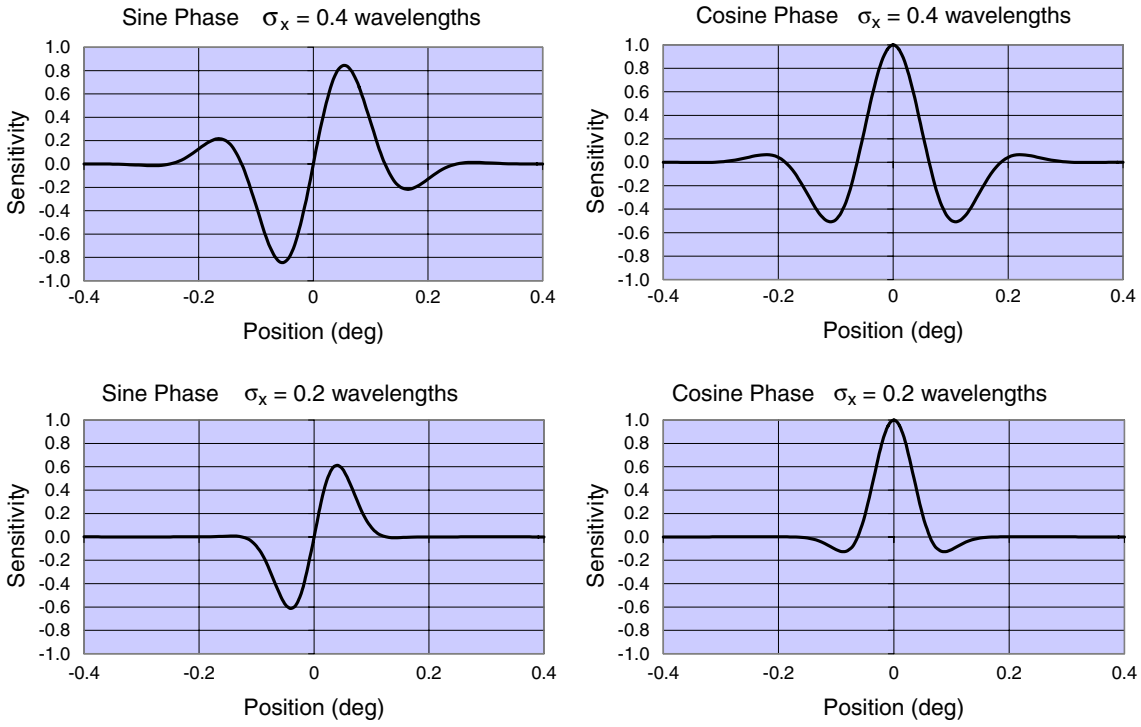

Fig. 8. Cross-sections of the sensitivity functions of sine and cosine receptive fields for two values of the standard deviation. These two standard deviations correspond approximately to the limits of the range consistent with our data and models. The standard deviation increases with the sparseness of the receptive field array.

Table 4 compares our estimates of size and shape with those of other studies that have used Gabor patterns as stimuli. All of them used detection tasks except Watson and Turano (1995), who used a direction discrimination task. These estimates vary greatly and the explanation for this variation is not clear. There were differences in the way that the estimates were made, and this likely accounts for some of the variance. We would expect bandwidth to decrease as frequency increases on the basis of evidence that the mean bandwidth of single striate cortex units decreases as their best frequency increases (DeValois, Albrecht, & Thorell, 1982). None of the other studies took account of the likely possibility that the threshold depends on more than one receptive field, a factor that we have shown to reduce the estimated size of the fields.

It is of interest to compare our model receptive fields with measurements of receptive fields in animals. Single unit studies of macaque striate cells showed them to have a wide range of bandwidths from about 0.4 to more than 2.6 octaves and averaging about 1.4 octaves (DeValois et al., 1982). Ringach (2002) used a reverse correlation method to determine the two-dimensional sensitivity functions of V1 receptive fields. He found that the receptive fields are well described by Gabor functions, as had been proposed earlier by Marcelja (1980). Ringach found that there was considerable variation in size and bandwidth, but most of the cells had standard deviations of less than

Table 4
Estimates of the size and shape of receptive fields from experiments using Gabor patterns

	Spatial frequency	Ratio σ_y/σ_x		Standard deviation	Full-width at 0.5 max	Full-width at 1/*e* max	Full equivalent width	Full bandwidth at 0.5 max	Full bandwidth at 0.5 max
	c/deg			σ_x Cycles	W_x Cycles 2.35 σ_x	2a Cycles 2.828 σ_x	Q Cycles 2.507 σ_x	W_f c/deg .8825*f/W_x	Octaves
Watson et al. (1983)	8.0	1		1.0608	2.493	3.000	2.659	2.832	0.516
Anderson and Burr (1991)	0.1	1		0.0600	0.141	0.170	0.150	0.626	Uncomputable
	10.0	1		0.2600	0.611	0.735	0.652	14.444	2.632
Watson and Turano (1995)	3.0	1		0.5266	1.238	1.489	1.320	2.139	1.076
Polat and Tyler (1999)	4.0	6.5	Coll.	2.7660	6.500	7.822	6.934	–	–
	4.0		Orth.	0.4256	1.000	1.204	1.067	3.529	1.367
Foley et al. (2006) (present paper)	4.0	1.2	Max.	0.4000	0.940	1.131	1.003	3.755	1.470
	4.0		Min.	0.2000	0.470	0.566	0.501	7.511	4.986

Please cite this article in press as: Foley, J. M. et al., Detection of Gabor patterns of different sizes, ..., *Vision Research* (2006), doi:10.1016/j.visres.2006.09.005

0.5 wavelength. Many were approximately circular with a tendency to be slightly elliptical with the longer axis collinear with the stripes. Mean $\sigma_x = 0.33$ wavelengths; mean $\sigma_y = 0.44$ wavelengths. Cells were tuned to the whole range of phases, with phases near 0, 90, 180, and 270 deg being more frequent than intermediate phases. This phase difference had not been found in earlier studies. There was also a tendency for receptive fields tuned to sine phase to be larger than those tuned to other phases. Ringach points out that these receptive fields are more varied and on average smaller than those predicted by models of efficient natural image coding. Similar receptive fields have been reported in area 17 of the cat (Jones & Palmer, 1987).

We conclude that the detection of our 4 c/deg vertical Gabor patterns is well described by a deterministic model in which the patterns stimulate an array of closely spaced linear receptive fields whose sensitivity functions are two-dimensional Gabor functions. The receptive fields have standard deviations of 0.2–0.4 wavelengths and are 10–50% longer in the direction collinear to the stripes and their sensitivity decreases as an exponential function of eccentricity. Mechanism responses are power functions of the excitation of the receptive fields with powers of about 2.5 and 3.1 for our two observers. Detection of all except the smallest patterns is mediated by a sum of responses over multiple receptive fields. The data are equally consistent with an internal-noise-limited model. The function relating the standard deviation of the decision variable trades-off with the value of m, and our data are insufficient to separate these two factors. However, the fact that mixing sizes in a stimulus sequence does not increase thresholds suggests that the limiting noise does not depend on the expected size of the stimulus.

Acknowledgments

This study was supported by National Eye Institute Grant EY12734. We thank Craig Abbey, Miguel Eckstein, and two anonymous reviewers for valuable comments on an earlier version of the paper.

Appendix A. Symbols used in the article

x, y	coordinates of a point re the fixation point specified in deg of visual angle
Stimulus pattern	
$c(x, y)$	contrast of the pattern as a function of x and y
x_s, y_s	horizontal and vertical coordinates of the pattern center
σ_{xs}, σ_{ys}	standard deviations of the stimulus pattern in the horizontal and vertical directions
f_s	spatial frequency of the underlying sinewave (c/deg)
ϕ_s	spatial phase of the underlying sinewave re the origin (rad)
C	contrast parameter of the pattern
C_t	value of the contrast parameter of the pattern at threshold (target contrast threshold)
Receptive field	
$s(x, y)$	sensitivity of the receptive field as a function of x and y
x_f, y_f	horizontal and vertical coordinates of the receptive field center
σ_{xf}, σ_{yf}	standard deviations of the receptive field in the horizontal and vertical directions
f_f	spatial frequency of the underlying sinewave
ϕ_f	spatial phase of the underlying sinewave re the origin
S	sensitivity parameter of the receptive field
Model	
S_0	sensitivity parameter of the receptive field centered on the stimulus
k	parameter of threshold vs. eccentricity function
a	factor by which sensitivity parameter decreases for each wavelength of eccentricity
d_j	distance from fixation point to center of receptive field j in wavelengths
F_{ij}	symbol for the expression after S in Appendix C, Eq. (C17) for pattern i and receptive field, j
E_{ij}	excitation of a receptive field j by pattern i
E'_{ij}	effective excitation of receptive field j by pattern i
s_{ij}	sensitivity of receptive field j to pattern i
s'_{ij}	effective sensitivity of receptive field j to pattern i
R_j	response of mechanism j
D_i	detection variable
m	power to which excitation is raised to produce the response of the mechanism
d'_i	decision variable in noise limited model
σ_i	standard deviation of decision variable
i	index for pattern
j	index for receptive field

Appendix B. Contrast energy of Gabor patterns

The contrast function of a vertical luminance spatial Gabor pattern centered at 0, 0 is described by the following equation:

$$c(x, y) = C \exp\left(-\frac{x^2}{2\sigma_x^2} - \frac{y^2}{2\sigma_y^2}\right) \sin\left(\frac{2\pi}{\lambda}x + \phi\right) f(t), \qquad \text{(B1)}$$

where x and y are the horizontal and vertical coordinates of a point, C, λ, and ϕ are the contrast, wavelength, and spatial phase (re 0, 0) of the sinewave, σ_x and σ_y are the standard deviations of the Gaussian envelope, and $f(t)$ is the temporal envelope. All spatial dimensions are usually specified as visual angles. When $\phi = 0$ deg, we have positive sine phase in which a bright stripe appears to the right

of the center of the pattern and when $\phi = 180$ deg we have negative sine phase in which the bright band appears to the left of the center. Similarly when $\phi = 90$ deg, we have positive cosine phase in which there is a bright stripe in the center of the pattern and when $\phi = 270$ deg, we have negative cosine phase in which there is a dark stripe in the center. We will consider the case where the pattern has a rectangular temporal envelope, so that $f(t) = 1$ during the interval when the pattern is on and 0 otherwise.

Contrast energy is defined as the squared integral of the pattern:

$$\varepsilon = \int_{-\infty}^{\infty} dy \int_{-\infty}^{\infty} dx c(x,y)^2. \tag{B2}$$

The following steps show the derivation of the expression for the contrast energy:

$$\varepsilon = C^2 \int_{-\infty}^{\infty} dy \int_{-\infty}^{\infty} dx \times \exp\left(-\frac{x^2}{\sigma_x^2} - \frac{y^2}{\sigma_y^2}\right) \sin^2\left(\frac{2\pi}{\lambda}x + \phi\right) \int_0^T dt, \tag{B3}$$

where T is the duration of the pattern in seconds.

Using the trigonometric identity, $\cos 2\theta = 1 - 2\sin^2\theta$ and solving the time integral, we get,

$$\varepsilon = \frac{C^2}{2} T \int_{-\infty}^{\infty} dy \exp\left(-\frac{y^2}{\sigma_y^2}\right) \int_{-\infty}^{\infty} dx \exp\left(-\frac{x^2}{\sigma_x^2}\right)\left[1 - \cos\left(\frac{4\pi}{\lambda}x + 2\phi\right)\right]. \tag{B4}$$

Let $I_y = \int_{-\infty}^{\infty} dy \exp\left(-\frac{y^2}{\sigma_y^2}\right)$, and $I_x = \int_{-\infty}^{\infty} dx \exp\left(-\frac{x^2}{\sigma_x^2}\right)$. Therefore, Eq. (B4) becomes,

$$\varepsilon = \frac{C^2}{2} T I_y \left[I_x - \int_{-\infty}^{\infty} dx \exp\left(-\frac{x^2}{\sigma_x^2}\right) \cos\left(\frac{4\pi}{\lambda}x + 2\phi\right)\right]. \tag{B5}$$

First, let us determine the value of I_y:

$$I_y = \int_{-\infty}^{\infty} dy \exp\left(-\frac{y^2}{\sigma_y^2}\right). \tag{B6}$$

We know that

$$\int_{-\infty}^{\infty} dy \exp\left(-ay^2\right) = \sqrt{\frac{\pi}{a}}. \tag{B7}$$

This implies that $a = \frac{1}{\sigma_y^2}$ yielding

$$\int_{-\infty}^{\infty} dy \exp\left(-\frac{y^2}{\sigma_y^2}\right) = I_y = \sqrt{\pi}\sigma_y. \tag{B8}$$

Similarly,

$$I_x = \sqrt{\pi}\sigma_x. \tag{B9}$$

To simplify the other integral in Eq. (B5) we make use of the trigonometric identity

$$\cos(A + B) = \cos(A)\cos(B) - \sin(A)\sin(B). \tag{B10}$$

Therefore,

$$\begin{aligned}\int_{-\infty}^{\infty} dx \exp\left(-\frac{x^2}{\sigma_x^2}\right) \cos\left(\frac{4\pi}{\lambda}x + 2\phi\right) &= \int_{-\infty}^{\infty} dx \exp\left(-\frac{x^2}{\sigma_x^2}\right)\left\{\cos\left(\frac{4\pi}{\lambda}x\right)\cos(2\phi) - \sin\left(\frac{4\pi}{\lambda}x\right)\sin(2\phi)\right\} \\ &= \cos(2\phi)\int_{-\infty}^{\infty} dx \exp\left(-\frac{x^2}{\sigma_x^2}\right)\cos\left(\frac{4\pi}{\lambda}x\right) - \sin(2\phi)\int_{-\infty}^{\infty} dx \exp\left(-\frac{x^2}{\sigma_x^2}\right)\sin\left(\frac{4\pi}{\lambda}x\right).\end{aligned} \tag{B11}$$

But,

$$\sin(2\phi)\int_{-\infty}^{\infty} dx \exp\left(-\frac{x^2}{\sigma_x^2}\right)\sin\left(\frac{4\pi}{\lambda}x\right) = 0,$$

since the integrand is an odd function. Therefore Eq. (B11) becomes,

$$\begin{aligned}\int_{-\infty}^{\infty} dx \exp\left(-\frac{x^2}{\sigma_x^2}\right) \cos\left(\frac{4\pi}{\lambda}x + 2\phi\right) &= \cos(2\phi)\int_{-\infty}^{\infty} dx \exp\left(-\frac{x^2}{\sigma_x^2}\right)\cos\left(\frac{4\pi}{\lambda}x\right) \\ &= \cos(2\phi)\sqrt{\pi}\sigma_x \exp\left(-\frac{4\pi^2\sigma_x^2}{\lambda^2}\right),\end{aligned} \tag{B12}$$

where we have used the known result

$$\int_{-\infty}^{\infty} dx \exp(-ax^2)\cos(bx) = \sqrt{\frac{\pi}{a}}\exp\left(-\frac{b^2}{4a}\right), \tag{B13}$$

in the second equality of Eq. (B12). Substituting Eqs. (B12), (B9) and (B8) in Eq. (B5), we obtain a general equation for the contrast energy of the class of vertical Gabor patterns considered here:

$$\varepsilon = \frac{C^2}{2} T\pi\sigma_x\sigma_y\left[1 - \cos(2\phi)\exp\left(-\frac{4\pi^2\sigma_x^2}{\lambda^2}\right)\right]. \tag{B14}$$

Appendix C. Excitation of a Gabor receptive field at any location by a Gabor pattern centered on the fixation point

Let the stimulus be a vertically oriented Gabor pattern centered at (x_s, y_s) with contrast C, pattern standard deviations σ_{xs} and σ_{ys}, and spatial frequency f_s, in ϕ_s phase with respect to its center. The contrast function of such a pattern is given by

$$c(x,y) = C\exp\left[-\frac{(x - x_s)^2}{2\sigma_{xs}^2} - \frac{(y - y_s)^2}{2\sigma_{ys}^2}\right] \times \sin\left(2\pi f_s(x - x_s) + \phi_s\right). \tag{C1}$$

The pattern is detected by a mechanism with a receptive field whose spatial sensitivity function, $s(x,y)$, is also described by a vertically oriented Gabor function centered at (x_f, y_f) with sensitivity parameter S, standard deviations,

σ_{xf} and σ_{yf}, spatial frequency f_f, and a phase of ϕ_f re the center of the receptive field:

$$s(x,y) = S\exp\left[-\frac{(x-x_f)^2}{2\sigma_{xf}^2}-\frac{(y-y_f)^2}{2\sigma_{yf}^2}\right] \times \sin(2\pi f_f(x-x_f)+\phi_f). \quad \text{(C2)}$$

Excitation of the mechanism by the pattern is defined as:

$$E=\int_{-\infty}^{\infty}dy\int_{-\infty}^{\infty}dx\,c(x,y)s(x,y)$$

$$E=CS\int_{-\infty}^{\infty}dy\int_{-\infty}^{\infty}dx \exp\left[-\frac{(x-x_s)^2}{2\sigma_{xs}^2}-\frac{(y-y_s)^2}{2\sigma_{ys}^2}-\frac{(x-x_f)^2}{2\sigma_{xf}^2}-\frac{(y-y_f)^2}{2\sigma_{yf}^2}\right] \times \sin(2\pi f_f(x-x_f)+\phi_f)\sin(2\pi f_s(x-x_s)+\phi_s), \quad \text{(C3)}$$

which can be rewritten as:

$$E = CS\int_{-\infty}^{\infty}dy\exp\left[-\frac{(y-y_s)^2}{2\sigma_{ys}^2}-\frac{(y-y_f)^2}{2\sigma_{yf}^2}\right] \times\int_{-\infty}^{\infty}dx\exp\left[-\frac{(x-x_s)^2}{2\sigma_{xs}^2}-\frac{(x-x_f)^2}{2\sigma_{xf}^2}\right] \times \sin(2\pi f_s(x-x_s)+\phi_s)\sin(2\pi f_f(x-x_f)+\phi_f). \quad \text{(C4)}$$

Let I_y be the first integral and I_x be the second integral.

$$I_y=\int_{-\infty}^{\infty}dy\exp\left[-\frac{(y-y_s)^2}{2\sigma_{ys}^2}-\frac{(y-y_f)^2}{2\sigma_{yf}^2}\right], \quad \text{(C5)}$$

$$I_x=\int_{-\infty}^{\infty}dx\exp\left[-\frac{(x-x_s)^2}{2\sigma_{xs}^2}-\frac{(x-x_f)^2}{2\sigma_{xf}^2}\right] \times \sin(2\pi f_s(x-x_s)+\phi_s)\sin(2\pi f_f(x-x_f)+\phi_f). \quad \text{(C6)}$$

Making the assumption that the Gaussian stimulus envelope is centered at $(0,0)$, (i.e., $x_s=0$ and $y_s=0$) Eq. (C5) becomes,

$$I_y=\int_{-\infty}^{\infty}dy\exp\left[-\frac{y^2}{2\sigma_{ys}^2}-\frac{(y-y_f)^2}{2\sigma_{yf}^2}\right] =\int_{-\infty}^{\infty}dy\exp\left[-\left(y^2\frac{\sigma_{yf}^2+\sigma_{ys}^2}{2\sigma_{ys}^2\sigma_{yf}^2}-y\frac{y_f}{\sigma_{yf}^2}+\frac{y_f^2}{2\sigma_{yf}^2}\right)\right]. \quad \text{(C7)}$$

Using the known identity

$$\int_{-\infty}^{\infty}dy\exp[-(ax^2+bx+c)]=\sqrt{\frac{\pi}{a}}\exp\left(\frac{b^2-4ac}{4a}\right), \quad \text{(C8)}$$

in Eq. (C7), we obtain

$$I_y=\sqrt{\frac{\pi}{\frac{\sigma_{yf}^2+\sigma_{ys}^2}{2\sigma_{yf}^2\sigma_{ys}^2}}}\exp\left(\frac{\left(\frac{y_f}{\sigma_{yf}^2}\right)^2-\left(\frac{\sigma_{yf}^2+\sigma_{ys}^2}{\sigma_{ys}^2\sigma_{yf}^2}\right)\left(\frac{y_f^2}{\sigma_{yf}^2}\right)}{2\left(\frac{\sigma_{yf}^2+\sigma_{ys}^2}{\sigma_{ys}^2\sigma_{yf}^2}\right)}\right).$$

After simplification we obtain

$$I_y=\sqrt{\frac{2\pi\sigma_{yf}^2\sigma_{ys}^2}{\sigma_{yf}^2+\sigma_{ys}^2}}\exp\left(\frac{y_f^2}{2\sigma_{yf}^2}\left(\frac{\sigma_{ys}^2}{\sigma_{ys}^2+\sigma_{yf}^2}-1\right)\right). \quad \text{(C9)}$$

To evaluate I_x we use the trigonometric identities:

$$\cos(A\pm B)=\cos(A)\cos(B)\mp\sin(A)\sin(B)$$
$$\sin(A\pm B)=\sin(A)\cos(B)\pm\cos(A)\sin(B)$$
$$2\sin(A)\sin(B)=\cos(A-B)-\cos(A+B)$$

Applying these to I_x, taking account of the fact that $x_s=0$:

$$\begin{aligned}&2\sin(2\pi f_s x+\phi_s)\sin(2\pi f_f(x-x_f)+\phi_f)\\ &=\cos[2\pi f_s x+\phi_s-2\pi f_f(x-x_f)-\phi_f]-\cos[2\pi f_s x\\ &\quad+\phi_s+2\pi f_f(x-x_f)+\phi_f]\\ &=\cos[2\pi x(f_s-f_f)+(\phi_s-\phi_f+2\pi f_f x_f)]-\cos[2\pi x(f_s+f_f)\\ &\quad+(\phi_s+\phi_f-2\pi f_f x_f)]\\ &=\cos[2\pi x(f_s-f_f)]\cos[\phi_s-\phi_f+2\pi f_f x_f]\\ &\quad-\sin[2\pi x(f_s-f_f)]\sin[\phi_s-\phi_f+2\pi f_f x_f]\\ &\quad-\cos[2\pi x(f_s+f_f)]\cos[(\phi_s+\phi_f-2\pi f_f x_f)]\\ &\quad+\sin[2\pi x(f_s+f_f)]\sin[(\phi_s+\phi_f-2\pi f_f x_f)]. \quad \text{(C10)}\end{aligned}$$

Substituting Eq. (C10) into Eq. (C6), we get

$$\begin{aligned}I_x=&\frac{1}{2}\int_{-\infty}^{\infty}dx\exp\left[-\frac{x^2}{2\sigma_{xs}^2}-\frac{(x-x_f)^2}{2\sigma_{xf}^2}\right]\\ &\cos(2\pi x(f_s-f_f))\cos(\phi_s-\phi_f+2\pi f_f x_f)\\ &-\frac{1}{2}\int_{-\infty}^{\infty}dx\exp\left[-\frac{x^2}{2\sigma_{xs}^2}-\frac{(x-x_f)^2}{2\sigma_{xf}^2}\right]\sin(2\pi x(f_s-f_f))\\ &\sin(\phi_s-\phi_f+2\pi f_f x_f)\\ &-\frac{1}{2}\int_{-\infty}^{\infty}dx\exp\left[-\frac{x^2}{2\sigma_{xs}^2}-\frac{(x-x_f)^2}{2\sigma_{xf}^2}\right]\cos(2\pi x(f_s+f_f))\\ &\cos(\phi_s+\phi_f-2\pi f_f x_f)\\ &+\frac{1}{2}\int_{-\infty}^{\infty}dx\exp\left[-\frac{x^2}{2\sigma_{xs}^2}-\frac{(x-x_f)^2}{2\sigma_{xf}^2}\right]\sin(2\pi x(f_s+f_f))\\ &\sin(\phi_s+\phi_f-2\pi f_f x_f). \quad \text{(C11)}\end{aligned}$$

The second and fourth terms (integrals) in the above expression for I_x equal zero (because the integrands are odd function and the integral limits are symmetric). Therefore, we have,

$$\begin{aligned}I_x=&\frac{1}{2}\int_{-\infty}^{\infty}dx\exp\left[-\left(x^2\frac{\sigma_{xf}^2+\sigma_{xs}^2}{2\sigma_{xs}^2\sigma_{xf}^2}-x\frac{x_f}{\sigma_{xf}^2}+\frac{x_f^2}{2\sigma_{xf}^2}\right)\right]\\ &\cos(2\pi x(f_s-f_f))\cos(\phi_s-\phi_f+2\pi f_f x_f),\\ &-\frac{1}{2}\int_{-\infty}^{\infty}dx\exp\left[-\left(x^2\frac{\sigma_{xf}^2+\sigma_{xs}^2}{2\sigma_{xs}^2\sigma_{xf}^2}-x\frac{x_f}{\sigma_{xf}^2}+\frac{x_f^2}{2\sigma_{xf}^2}\right)\right]\\ &\cos(2\pi x(f_s+f_f))\cos(\phi_s+\phi_f-2\pi f_f x_f). \quad \text{(C12)}\end{aligned}$$

It can be shown that[2]

$$I = \int_{-\infty}^{\infty} dx \exp[-(ax^2+bx+c)]\cos(kx)$$
$$= \sqrt{\frac{\pi}{a}}\exp\left[-c+\frac{b^2}{4a}\right]\cos\left(\frac{kb}{2a}\right)\exp\left[-\frac{k^2}{4a}\right]$$
$$= \sqrt{\frac{\pi}{a}}\exp\left[-c+\frac{b^2-k^2}{4a}\right]\cos\left(\frac{kb}{2a}\right)$$
$$= \sqrt{\frac{\pi}{a}}\exp\left[\frac{-4ac+b^2-k^2}{4a}\right]\cos\left(\frac{kb}{2a}\right). \quad \text{(C13)}$$

Applying this to Eq. (C12), for the two integrals we get:

$$\int_{-\infty}^{\infty} dx \exp\left[-\left(x^2\frac{\sigma_{xf}^2+\sigma_{xs}^2}{2\sigma_{xs}^2\sigma_{xf}^2} - x\frac{x_f}{\sigma_{xf}^2}+\frac{x_f^2}{2\sigma_{xf}^2}\right)\right]\cos(2\pi x(f_s-f_f))$$
$$= \sqrt{\frac{2\pi\sigma_{xs}^2\sigma_{xf}^2}{\sigma_{xf}^2+\sigma_{xs}^2}}\exp\left[\frac{-x_f^2-4\pi^2\sigma_{xs}^2\sigma_{xf}^2(f_s-f_f)^2}{2(\sigma_{xf}^2+\sigma_{xs}^2)}\right]$$
$$\times\cos\left[\frac{2\pi x_f\sigma_{xs}^2(f_s-f_f)}{(\sigma_{xf}^2+\sigma_{xs}^2)}\right], \quad \text{(C14)}$$

and

$$\int_{-\infty}^{\infty} dx \exp\left[-\left(x^2\frac{\sigma_{xf}^2+\sigma_{xs}^2}{2\sigma_{xs}^2\sigma_{xf}^2} - x\frac{x_f}{\sigma_{xf}^2}+\frac{x_f^2}{2\sigma_{xf}^2}\right)\right]\cos(2\pi x(f_s+f_f))$$
$$= \sqrt{\frac{2\pi\sigma_{xs}^2\sigma_{xf}^2}{\sigma_{xf}^2+\sigma_{xs}^2}}\exp\left[\frac{-x_f^2-4\pi^2\sigma_{xs}^2\sigma_{xf}^2(f_s+f_f)^2}{2(\sigma_{xf}^2+\sigma_{xs}^2)}\right]$$
$$\times\cos\left[\frac{2\pi x_f\sigma_{xs}^2(f_s+f_f)}{(\sigma_{xf}^2+\sigma_{xs}^2)}\right]. \quad \text{(C15)}$$

Substituting Eqs. (C14) and (C15) in Eq. (C12), we get,

$$I_x = \frac{1}{2}\sqrt{\frac{2\pi\sigma_{xs}^2\sigma_{xf}^2}{\sigma_{xf}^2+\sigma_{xs}^2}}\left\{\exp\left[\frac{-x_f^2-4\pi^2\sigma_{xs}^2\sigma_{xf}^2(f_s-f_f)^2}{2(\sigma_{xf}^2+\sigma_{xs}^2)}\right]\right.$$
$$\times\cos\left[\frac{2\pi x_f\sigma_{xs}^2(f_s-f_f)}{(\sigma_{xf}^2+\sigma_{xs}^2)}\right]\cos(\phi_s-\phi_f+2\pi f_f x_f)$$
$$-\exp\left[\frac{-x_f^2-4\pi^2\sigma_{xs}^2\sigma_{xf}^2(f_s+f_f)^2}{2(\sigma_{xf}^2+\sigma_{xs}^2)}\right]\cos\left[\frac{2\pi x_f\sigma_{xs}^2(f_s+f_f)}{(\sigma_{xf}^2+\sigma_{xs}^2)}\right]$$
$$\left.\times\cos(\phi_s+\phi_f-2\pi f_f x_f)\right\}. \quad \text{(C16)}$$

Substituting I_y, Eq. (C9) and I_x, Eq. (C16) in Eq. (C4), for the mechanism excitation we get:

$$E = CS\pi\sqrt{\frac{\sigma_{ys}^2\sigma_{yf}^2}{\sigma_{ys}^2+\sigma_{yf}^2}}\sqrt{\frac{\sigma_{xs}^2\sigma_{xf}^2}{\sigma_{xs}^2+\sigma_{xf}^2}}\exp\left(\frac{y_f^2}{2\sigma_{yf}^2}\left(\frac{\sigma_{ys}^2}{\sigma_{ys}^2+\sigma_{yf}^2}-1\right)\right)$$
$$\times\left\{\cos(\phi_s-\phi_f+2\pi f_f x_f)\right.$$
$$\times\exp\left[\frac{-x_f^2-4\pi^2\sigma_{xs}^2\sigma_{xf}^2(f_s-f_f)^2}{2(\sigma_{xs}^2+\sigma_{xf}^2)}\right]\cos\left(\frac{2\pi\sigma_{xs}^2x_f(f_s-f_f)}{\sigma_{xs}^2+\sigma_{xf}^2}\right)$$
$$-\cos(\phi_s+\phi_f-2\pi f_f x_f)\exp\left[\frac{-x_f^2-4\pi^2\sigma_{xs}^2\sigma_{xf}^2(f_s+f_f)^2}{2(\sigma_{xs}^2+\sigma_{xf}^2)}\right]$$
$$\left.\times\cos\left(\frac{2\pi\sigma_{xs}^2x_f(f_s+f_f)}{\sigma_{xs}^2+\sigma_{xf}^2}\right)\right\}. \quad \text{(C17)}$$

Thus, the excitation of a mechanism by a pattern is equal to the contrast parameter of the pattern, C_i, times the sensitivity parameter of the mechanism, S_j, times an expression that depends on both the pattern and the receptive field, F_{ij}:

$$E_{ij} = C_i S_j F_{ij}. \quad \text{(C18)}$$

We define C_t as the threshold contrast of the pattern. In the case in which a single mechanism mediates detection, we assume that at threshold, $E = 1$. Substituting these values in Eq. (C17) and solving for C_t we get:

---

[2] Derivation of Eq. (C13): Solution to the integral used in the analysis Eq. (C12). We start by completing the square of the quadratic term in the exponent

$$I = \int_{-\infty}^{\infty} dx \exp[-(ax^2+bx+c)]\cos[kx]$$
$$= \int_{-\infty}^{\infty} dx \exp\left[-\left(\left(\sqrt{a}x+\frac{b}{2\sqrt{a}}\right)^2+c-\frac{b^2}{4a}\right)\right]\cos[kx]$$
$$= \exp\left[-c+\frac{b^2}{4a}\right]\int_{-\infty}^{\infty} dx \exp\left[-\left(\sqrt{a}x+\frac{b}{2\sqrt{a}}\right)^2\right]\cos[kx].$$

Using a change of variable

$$y = \sqrt{a}x+\frac{b}{2\sqrt{a}} \quad \text{with} \quad dy = \sqrt{a}dx \quad \text{yields}$$
$$I = \exp\left[-c+\frac{b^2}{4a}\right]\frac{1}{\sqrt{a}}\int_{-\infty}^{\infty} dy \exp[-y^2]\cos\left[\frac{k}{\sqrt{a}}y-\frac{kb}{2a}\right].$$

Using the expression:

$$\cos(A-B) = \cos(A)\cos(B)+\sin(A)\sin(B),$$

we obtain for I:

$$I = \exp\left[-c+\frac{b^2}{4a}\right]\frac{1}{\sqrt{a}}\int_{-\infty}^{\infty} dy \exp[-y^2]\cos\left(\frac{k}{\sqrt{a}}y\right)\cos\left(\frac{kb}{2a}\right)$$
$$-\exp\left[-c+\frac{b^2}{4a}\right]\frac{1}{\sqrt{a}}\int_{-\infty}^{\infty} dy \exp[-y^2]\sin\left(\frac{k}{\sqrt{a}}y\right)\sin\left(\frac{kb}{2a}\right).$$

Because the second term is an odd function and the limits are symmetric, we obtain:

$$I = \exp\left[-c+\frac{b^2}{4a}\right]\cos\left(\frac{kb}{2a}\right)\frac{1}{\sqrt{a}}\int_{-\infty}^{\infty} dy \exp[-y^2]\cos\left(\frac{k}{\sqrt{a}}y\right).$$

Given

$$\int_{-\infty}^{\infty} dx \exp[-ax^2]\cos[bx] = \sqrt{\frac{\pi}{a}}\exp\left(-\frac{b^2}{4a}\right),$$

we obtain:

$$I = \exp\left[-c+\frac{b^2}{4a}\right]\cos\left(\frac{kb}{2a}\right)\sqrt{\frac{\pi}{a}}\exp\left(-\frac{k^2}{4a}\right).$$

$$C_t = \left[S\pi \sqrt{\frac{\sigma_{ys}^2\sigma_{yf}^2}{\sigma_{ys}^2+\sigma_{yf}^2}} \sqrt{\frac{\sigma_{xs}^2\sigma_{xf}^2}{\sigma_{xs}^2+\sigma_{xf}^2}} \exp\left(\frac{y_f^2}{2\sigma_{yf}^2}\left(\frac{\sigma_{ys}^2}{\sigma_{ys}^2+\sigma_{yf}^2}-1\right)\right) \times \left\{ \cos(\phi_s-\phi_f+2\pi f_f x_f)\exp\left[\frac{-x_f^2-4\pi^2\sigma_{xs}^2\sigma_{xf}^2(f_s-f_f)^2}{2(\sigma_{xs}^2+\sigma_{xf}^2)}\right] \times \cos\left(\frac{2\pi\sigma_{xs}^2 x_f(f_s-f_f)}{\sigma_{xs}^2+\sigma_{xf}^2}\right) - \cos(\phi_s+\phi_f-2\pi f_f x_f) \times \exp\left[\frac{-x_f^2-4\pi^2\sigma_{xs}^2\sigma_{xf}^2(f_s+f_f)^2}{2(\sigma_{xs}^2+\sigma_{xf}^2)}\right] \cos\left(\frac{2\pi\sigma_{xs}^2 x_f(f_s+f_f)}{\sigma_{xs}^2+\sigma_{xf}^2}\right) \right\} \right]^{-1}. \quad \text{(C19)}$$

The reciprocal of C_t is the sensitivity of the receptive field to the stimulus, S_{ij}.

Contrast thresholds can be transformed into contrast energy thresholds as follows:

The contrast energy of the circular Gabor pattern when it is at threshold is given by Eq. (B14) in Appendix B.

$$\varepsilon = \frac{C^2}{2} T\pi\sigma_{xs}\sigma_{ys}\left[1-\cos(2\phi_s)\exp\left(-\frac{4\pi^2\sigma_{xs}^2}{\lambda^2}\right)\right]. \quad \text{(C20)}$$

Substituting C_t for C and defining ε_t as the energy of the target pattern at threshold, we get:

$$\varepsilon_t = \frac{C_t^2}{2} T\pi\sigma_{xs}\sigma_{ys}\left[1-\cos(2\phi_s)\exp\left(-\frac{4\pi^2\sigma_{xs}^2}{\lambda^2}\right)\right]. \quad \text{(C21)}$$

To determine contrast energy at threshold predicted by the model, substitute the expression for C_t from Eq. (C19) in Eq. (C21).

Appendix D. Supplementary data

Supplementary data associated with this article can be found, in the online version, at doi:10.1016/j.visres.2006.09.005.

References

Anderson, S. J., & Burr, D. C. (1991). Spatial summation properties of directionally selective mechanisms in human vision. *Journal of the Optical Society of America a – Optics Image Science and Vision, 8*(8), 1330–1339.

Blakemore, C. B., & Campbell, F. W. (1969). On the existence of neurones in the human visual system selectively sensitive to the orientation and size of retinal images. *Journal of Physiology, 203*, 237–260.

Chen, C. C., & Tyler, C. W. (2001). Lateral sensitivity modulation explains the flanker effect in contrast discrimination. *Proceedings of the Royal Society of London Series B – Biological Sciences, 268*(1466), 509–516.

DeValois, R. L., Albrecht, D. G., & Thorell, L. G. (1982). Spatial-frequency selectivity of cells in Macaque visual-cortex. *Vision Research, 22*(5), 545–559.

Foley, J. M. (1994). Human luminance pattern-vision mechanisms – Masking experiments require a new model. *Journal of the Optical Society of America a – Optics Image Science and Vision, 11*(6), 1710–1719.

Foley, J. M., & Chen, C. C. (1997). Analysis of the effect of pattern adaptation on pattern pedestal effects: a two-process model. *Vision Research, 37*(19), 2779–2788.

Foley, J. M., & Chen, C.-C. (1999). Pattern detection in the presence of maskers that differ in spatial phase and temporal offset: Threshold measurements and a model. *Vision Research, 39*(23), 3855–3872.

Foley, J. M., & Legge, G. E. (1981). Contrast detection and near-threshold discrimination in human vision. *Vision Research, 21*(7), 1041–1053.

Foley, J. M., & Schwarz, W. (1998). Spatial attention: effect of position uncertainty and number of distractor patterns on the threshold-versus-contrast function for contrast discrimination. *Journal of the Optical Society of America a – Optics Image Science and Vision, 15*(5), 1036–1047.

Garcia-Perez, M. A., & Sierra-Vazquez, V. (1996). Do channels shift their tuning towards lower spatial frequencies in the periphery? *Vision Research, 36*(20), 3339–3372.

Georgeson, M. A., & Harris, M. G. (1984). Spatial selectivity of contrast adaptation: Models and data. *Vision Research, 24*, 729–741.

Graham, N. V. S. (1989). Visual pattern analyzers. Oxford psychology series; no. 16. (pp. xvi, 646). New York: Oxford University Press.

Graham, C. H., Brown, R. H., & Mote, F. A. (1939). The relation of size of stimulus and intensity in the human eye: II. Intensity thresholds for white light. *Journal of Experimental Psychology, 24*, 555–573.

Graham, N., & Robson, J. G. (1987). Summation of very close spatial frequencies: The importance of spatial probability summation. *Vision Research, 27*, 1997–2007.

Green, D. M., & Swets, J. A. (1966). *Signal detection theory and psychophysics*. New York: Wiley.

Hauske, G., Wolf, W., & Lupp, U. (1976). Matched-filters in human-vision. *Biological Cybernetics, 22*(4), 181–188.

Hines, M. (1976). Line spread function variation near the fovea. *Vision Research, 16*, 567–572.

Jones, J. P., & Palmer, L. A. (1987). An evaluation of the two-dimensional Gabor filter model of simple receptive-fields in cat striate cortex. *Journal of Neurophysiology, 58*(6), 1233–1258.

Kersten, D. (1984). Spatial summation in visual noise. *Vision Research, 24*(12), 1977–1990.

Khuri, A. A., & Cornell, J. A. (1987). *Response surfaces: designs and analysis*. New York: Dekker.

Kontsevich, L. L., Chen, C. C., & Tyler, C. W. (2002). Separating the effects of response nonlinearity and internal noise psychophysically. *Vision Research, 42*(14), 1771–1784.

Legge, G. E., & Foley, J. M. (1980). Contrast masking in human-vision. *Journal of the Optical Society of America, 70*(12), 1458–1471.

Marcelja, S. (1980). Mathematical-description of the responses of simple cortical-cells. *Journal of the Optical Society of America, 70*(11), 1297–1300.

Meese, T. S., Hess, R. F., & Williams, C. B. (2005). Size matters, but not for everyone: Individual differences for contrast discrimination. *Journal of Vision, 5*(11), 928–947.

Pointer, J. S., & Hess, R. F. (1989). The contrast sensitivity gradient across the human visual-field : with emphasis on the low spatial-frequency range. *Vision Research, 29*(9), 1133–1151.

Polat, U., & Tyler, C. W. (1999). What pattern the eye sees best. *Vision Research, 39*(5), 887–895.

Quick, R. F. (1974). A vector magnitude model of contrast detection. *Kybernetic, 16*, 65–67.

Ringach, D. L. (2002). Spatial structure and symmetry of simple-cell receptive fields in macaque primary visual cortex. *Journal of Neurophysiology, 88*(1), 455–463.

Robson, J. G., & Graham, N. (1981). Probability summation and regional variation in contrast sensitivity across the visual-field. *Vision Research, 21*(3), 409–418.

Rousseeuw, P. J. (1991). Tutorial to robust statistics. *Journal of Chemometrics, 5*, 1–20.

Rovamo, J., Luntinen, O., & Nasanen, R. (1993). Modelling the dependence of contrast sensitivity on grating area and spatial frequency. *Vision Research, 33*(18), 2773–2788.

Syvajarvi, A., Nasanen, R., & Rovamo, J. (1999). Spatial integration of signal information in Gabor stimuli. *Ophthalmic and Physiological Optics, 19*(3), 242–252.

Torgerson, W. S. (1958). *Theory and methods of scaling*. New York: Wiley.

Tyler, C. W., & Chen, C. C. (2000). Signal detection theory in the 2AFC paradigm: attention, channel uncertainty and probability summation. *Vision Research, 40*(22), 3121–3144.

Varadharajan, S. L., & Foley, J. M. (2003). Effects of flanking patterns on contrast detection and contrast discrimination [Abstract]. *Journal of Vision*, *3*(9), 345a, <http://journalofvision.org/3/9/345/>, doi:10.1167/3.9.345.

Warren, R. M., & Warren, R. P. (1968). *Helmholtz on perception: its physiology and development*. New York: Wiley.

Watson, A. B., & Ahumada, A. (2005). A standard model for foveal detection of spatial contrast. *Journal of Vision, 5*, 717–740.

Watson, A. B., Barlow, H. B., & Robson, J. G. (1983). What does the eye see best? *Nature, 302*(5907), 419–422.

Watson, A. B., & Pelli, D. G. (1983). Quest – a Bayesian Adaptive Psychometric Method. *Perception & Psychophysics, 33*(2), 113–120.

Watson, A. B., & Robson, J. G. (1981). Discrimination at threshold: labelled detectors in human vision. *Vision Research, 21*(7), 1115–1122.

Watson, A. B., & Turano, K. (1995). The optimal motion stimulus. *Vision Research, 35*(3), 325–336.

Westheimer, G. (1967). Spatial interaction in human cone vision. *Journal of Physiology – London, 190*, 139–154.

Wilson, H. R., McFarlane, D. K., & Phillips, G. C. (1983). Spatial frequency tuning of orientation selective units estimated by oblique masking. *Vision Research, 23*(9), 873–882.

Yu, C., Klein, S. A., & Levi, D. M. (2003). Cross- and Iso-oriented surrounds modulate the contrast response function: The effect of surround contrast. *Journal of Vision, 3*(8), 527–540.

Yu, C., & Levi, D. M. (1997). End stopping and length tuning in psychophysical spatial filters. *Journal of the Optical Society of America a – Optics Image Science and Vision, 14*(9), 2346–2354.

Yu, C., & Levi, D. M. (1998). Spatial-frequency and orientation tuning in psychophysical end-stopping. *Visual Neuroscience, 15*(4), 585–595.

Please cite this article in press as: Foley, J. M. et al., Detection of Gabor patterns of different sizes, ..., *Vision Research* (2006), doi:10.1016/j.visres.2006.09.005